Thymic macrophages consist of two populations with distinct localization and origin

Tyng-An Zhou[1], Hsuan-Po Hsu[1], Yueh-Hua Tu[2,3], Chih-Yu Lin[1], Nien-Jung Chen[1], Jin-Wu Tsai[4], Ellen A. Robey[5], Hsuan-Cheng Huang[2,6], Chia-Lin Hsu[1], and Ivan L. Dzhagalov[1*]

[1]Institute of Microbiology and Immunology, National Yang-Ming University, Taipei, Taiwan

[2]Bioinformatics Program, Taiwan International Graduate Program, Institute of Information Science, Academia Sinica, Taipei, Taiwan

[3]Graduate Institute of Biomedical Electronics and Bioinformatics, National Taiwan University, Taipei, Taiwan

[4]Brain Research Center, National Yang-Ming University, Taipei, Taiwan

[5]Division of Immunology and Pathogenesis, Department of Molecular and Cell Biology, University of California, Berkeley, CA, United States

[6]Institute of Biomedical Informatics, National Yang-Ming University, Taipei, Taiwan

*Correspondence to Ivan L. Dzhagalov: ivan.dzhagalov@nycu.edu.tw, ORCID: 0000-0001-9209-4582

Mailing Address: Ivan L. Dzhagalov, Institute of Microbiology and Immunology, National Yang-Ming Chiao-Tung University, #155, Sec. 2, LiNong Street, Beitou, Taipei City, 11221, TAIWAN

Abstract

Tissue-resident macrophages are essential for protection from pathogen invasion and maintenance of organ homeostasis. The ability of thymic macrophages to engulf apoptotic thymocytes is well appreciated, but little is known about their ontogeny, maintenance, and diversity. Here, we characterized the surface phenotype and transcriptional profile of these cells and found out that they express typical tissue-resident macrophage genes yet also exhibit organ-specific features. Thymic macrophages were most closely related to spleen red pulp macrophages and Kupffer cells and shared the expression of the transcription factor SpiC with these cells. Using shield chimeras, transplantation of embryonic thymuses, and fate mapping, we found that three distinct waves of precursors generate thymic macrophages. Moreover, some of them proliferated in situ. Single-cell RNA sequencing showed that the macrophages in the adult thymus are composed of two populations with distinct localization and origin. Altogether, our work defines the phenotype, origin, and diversity of thymic macrophages.

Introduction

Tissue-resident macrophages are present in every organ and maintain local homeostasis through diverse functions ranging from protection against pathogens to tissue repair[1]. To perform their roles efficiently, macrophages acquire specialized phenotypes depending on the tissue microenvironment, and as a consequence, multiple subtypes exist, frequently within the same organ. For example, the spleen harbors red pulp macrophages specialized in red blood cell phagocytosis, marginal zone macrophages and metallophilic macrophages that are the first defense against blood-borne pathogens, T cell zone macrophages that silently dispose of apoptotic immune cells, and tingible-body macrophages that engulf less fit B cells in the germinal center[2-4]. Thus, tissue-resident macrophages represent a fascinating developmental system that allows enormous plasticity.

The last decade has seen a paradigm shift in our understanding of the development of tissue-resident macrophages. Contrary to the long-held belief that all macrophages derive from circulating monocytes[5], multiple studies have shown that many of them are long-lived cells with an embryonic origin that can maintain themselves in the tissues (reviewed in[6]). Three waves of distinct progenitors settle the tissues and contribute in various degrees to the resident macrophages in each organ. The first wave consists of yolk sac (YS)-derived primitive macrophages that enter all tissues and establish the earliest macrophage populations[7,8]. In all organs, except for the brain and, partially, the epidermis, primitive macrophages are replaced by the next wave consisting of fetal monocytes[9-12]. The third wave comes from hematopoietic stem cell (HSC)-derived monocytes that contribute to various degrees to the

macrophage pool in different tissues. For example, these cells contribute little to the microglia in the brain, Langerhans cells in the epidermis, and alveolar macrophages in the lungs but substantially to most other organs[13-16]. Moreover, the kinetics and timing of HSC-derived monocytes infiltration vary in different parts of the body. For some macrophage populations, such as the arterial macrophages and subcapsular lymph node macrophages, monocytes replace embryonic macrophages soon after birth and self-maintain after that with little contribution from circulating cells[17,18]. Others, such as heart macrophages, osteoclasts, and pancreatic isles macrophages are progressively replaced at a low rate[14,19-23]. A third group, such as the macrophages in the dermis and most of the gut macrophages, are constantly replaced by blood monocytes with relatively fast kinetics[24,25]. These conclusions have been extended to many different macrophage populations such as Kupffer cells, liver capsular macrophages, red pulp macrophages, testicular macrophages, large and small peritoneal macrophages, and T zone macrophages in the lymph nodes[2,13,14,16,26-30].

The recent revitalization in macrophage research has yet to reach thymic macrophages. Although their prodigious phagocytic ability is well appreciated[31], little is known about the origin, diversity, and maintenance of these cells. This gap in our knowledge is, in part, due to the lack of a consensus about the surface phenotype of thymic macrophages. Various groups have used different markers to identify these cells, such as F4/80 and Mac-3 (LAMP-2)[31], or CD4 and CD11b[32], or Mac-2 (galectin 3), F4/80 and ED-1 (CD68)[33]. Most commonly, researchers employ F4/80 and CD11b[34-37]. However, none of these markers is macrophage-specific: F4/80 is also

91 expressed on eosinophils and monocytes[38,39], while CD11b is present on
92 most myeloid cells. The lack of a clear phenotypic definition of thymic
93 macrophages has translated into the absence of models that target genes
94 specifically in this population. For example, although macrophages in various
95 organs have been successfully targeted with *Lyz2*^{Cre}, *Csf1r*^{Cre}, or *Cx3cr1*^{Cre},
96 very few studies have used these models in the thymus[37,40,41].
97 Only a handful of studies has explored the origin of thymic macrophages.
98 Several reports have indicated that these cells could be derived from T cell
99 progenitors in the thymus based on an improved single cell in vitro culture and
100 in vivo transplantation experiments[42,43]. However, these conclusions have
101 been questioned based on fate-mapping experiments using *Il7r*^{Cre} that found
102 very limited contribution of lymphoid progenitors to thymic macrophages in
103 vivo in unperturbed mice[44]. Most recently, Tacke et al. used parabiosis to
104 rule out circulating monocytes as a major source for thymic macrophages[37].
105 The same study also performed fate-mapping experiments to show that most
106 thymic macrophages descend from *Flt3*$^{+}$ HSC-derived progenitors. However,
107 the contribution of earlier waves of hematopoiesis has not been explored.
108 Here, we aimed to bring our knowledge of thymic macrophages on par with
109 other tissue-resident macrophages. We started by providing a clear definition
110 of thymic macrophages according to the guidelines set by the Immunological
111 Genome Consortium (IMMGEN)[38] and characterized their surface
112 phenotype and transcriptional signature. Using single-cell RNA sequencing
113 (scRNA-Seq), we identified two populations of thymic macrophages with
114 distinct localization. We explored the origin of these cells through genetic fate
115 mapping, shield chimeras, and embryonic thymus transplantation and

116 documented that three separate waves of progenitors give rise to resident
117 thymic macrophages. Altogether our work fills an important gap in our
118 understanding of resident thymic macrophages and provides the framework
119 for future functional characterization of these cells.
120
121 **Results:**
122 **CD64, F4/80, and MerTK identify the macrophages in the thymus**
123 To unambiguously and comprehensively identify macrophages in the
124 thymus, we evaluated several of the prototypical macrophage markers,
125 MerTK, CD64, and F4/80[38]. Only MerTK identified a population that stained
126 completely with the other two markers (Fig. 1a). F4/80 labeled Siglec $F^{+}SSC^{hi}$
127 eosinophils and $CD64^{+}CD11b^{+}$ monocytes, in addition to $MerTK^{+}$ cells (Fig.
128 S1a). CD64 identified $CD11b^{+}F4/80^{lo}$ monocytes (Fig. S1b). Thus, MerTK
129 appeared to be the best marker for macrophages in the thymus. However,
130 staining with MerTK and F4/80 was relatively dim even when the brightest
131 fluorochromes (e.g., PE) were used and could not be resolved fully from the
132 isotype control (Fig. S1c). For practical purposes, to identify macrophages,
133 we used CD64 together with F4/80 and CD11b to exclude monocytes (Fig.
134 S1d). In addition, we also employed forward scatter (cells size) to exclude
135 cells that appeared $MerTK^{+}$, $CD64^{+}$, $F4/80^{+}$, but were much smaller and less
136 granular than the rest of the macrophages, and many of them were $Thy1^{+}$
137 (Fig. S1e).
138 The $CD64^{+}F4/80^{+}MerTK^{+}CD11b^{lo}FSC^{hi}$ cells had typical macrophage
139 morphology with abundant cytoplasm (Fig. 1b). These cells did not express
140 lineage markers characteristic of T cells (CD3ε), B cells (CD19), eosinophils

141 (Siglec F), NK cells (NK1.1), neutrophils (Gr1), or plasmacytoid dendritic cells
142 (Siglec H) (Fig. 1c). However, they expressed phagocytic receptors such as
143 TIM4, CD51, and Axl (Fig. 1d).

144 To ascertain that our gating strategy identifies all macrophages in the
145 thymus in an unbiased way, we performed scRNA-Seq of sorted *Csf1r*$^{GFP+}$
146 and *Cd11c*$^{YFP+}$ thymic cells. *Csf1r* is required for the survival of most
147 macrophages and is considered their definitive marker[45,46], while *Cd11c*^{YFP}
148 is expressed in many myeloid cells, including macrophages[47]. Both
149 reporters identified an overlapping set of cells (Fig. S2a). Two clusters
150 expressed the macrophage/monocytes-specific transcription factor *Mafb* and
151 high levels of *Fcrg1* (CD64), *Mertk*, and *Adgre1* (F4/80), indicating that they
152 are macrophages (Fig. 1e). An additional cluster expressed *Mafb* together
153 with *Fcgr1* and *Adgre1* but not *Mertk*, fitting the description of monocytes.
154 Altogether the scRNA-Seq data confirmed that our flow cytometry gating had
155 identified all macrophages in the thymus. Importantly, MerTK^{+} cells could not
156 be labeled by intravenously injected CD45 antibody (Fig. 1f), proving that they
157 reside in the parenchyma of the organs and not in the blood vessels. Based
158 on the above data, we will refer to CD64^{+}F4/80^{+}MerTK^{+}CD11b^{lo}FSC^{hi} cells as
159 thymic macrophages. The smaller CD64^{+}F4/80^{lo}CD11b^{+}FSC^{hi} population did
160 not express MerTK, but most of them expressed Ly6C, and we classify them
161 as thymic monocytes.

162 Thymic macrophages expressed CD11c, MHC2, and SIRPα that made
163 them partially overlap with CD11c^{+}MHC2^{+} classical dendritic cells (cDCs),
164 thus making problematic the unambiguous identification of thymic cDCs
165 based only on these two markers (Fig. S1f). Proper identification of cDC in the

166 thymus requires the exclusion of macrophages based on CD64 or MerTK
167 staining. Otherwise, the cDCs, particularly the SIRPα^+ cDC2 subset, would
168 be contaminated with macrophages that account for ~25% of cDC2 (Fig.
169 S1g).
170 Thymic macrophages were ~0.1% of all the cells in the thymus of young
171 adult mice and numbered ~4x10^5 on average per mouse (Fig. 1g). We did not
172 find statistically significant differences in their percentages between 4 and 11
173 weeks of age. Still, there was a significant decline in their numbers with age,
174 consistent with the beginning of thymic involution (Fig. 1h).
175 To determine if thymic macrophages are avid phagocytes, we evaluated
176 their participation in the phagocytosis of apoptotic cells in the thymus by
177 TUNEL staining. We used TIM4 and MerTK as single stains to identify
178 macrophages in tissue sections because they are not expressed on any other
179 cell type in the thymus instead of following our multiple-label flow cytometry
180 strategy. Most of the TUNEL$^+$ cells could be found clearly inside or closely
181 associated with MerTK$^+$ and TIM4$^+$ cells in the thymus (Fig. S3a and b). On
182 average, ~85% of all TUNEL$^+$ cells were within 5 μm of MerTK$^+$ cells,
183 indicating that thymic macrophages are the major phagocytic population in the
184 thymus (Fig. S3c). The degree of co-localization between TUNEL$^+$ cells and
185 TIM4$^+$ cells was slightly lower, ~75% on average, possibly reflecting the
186 absence of TIM4 expression on a small proportion of thymic macrophages
187 (Fig. 1d).

188

189

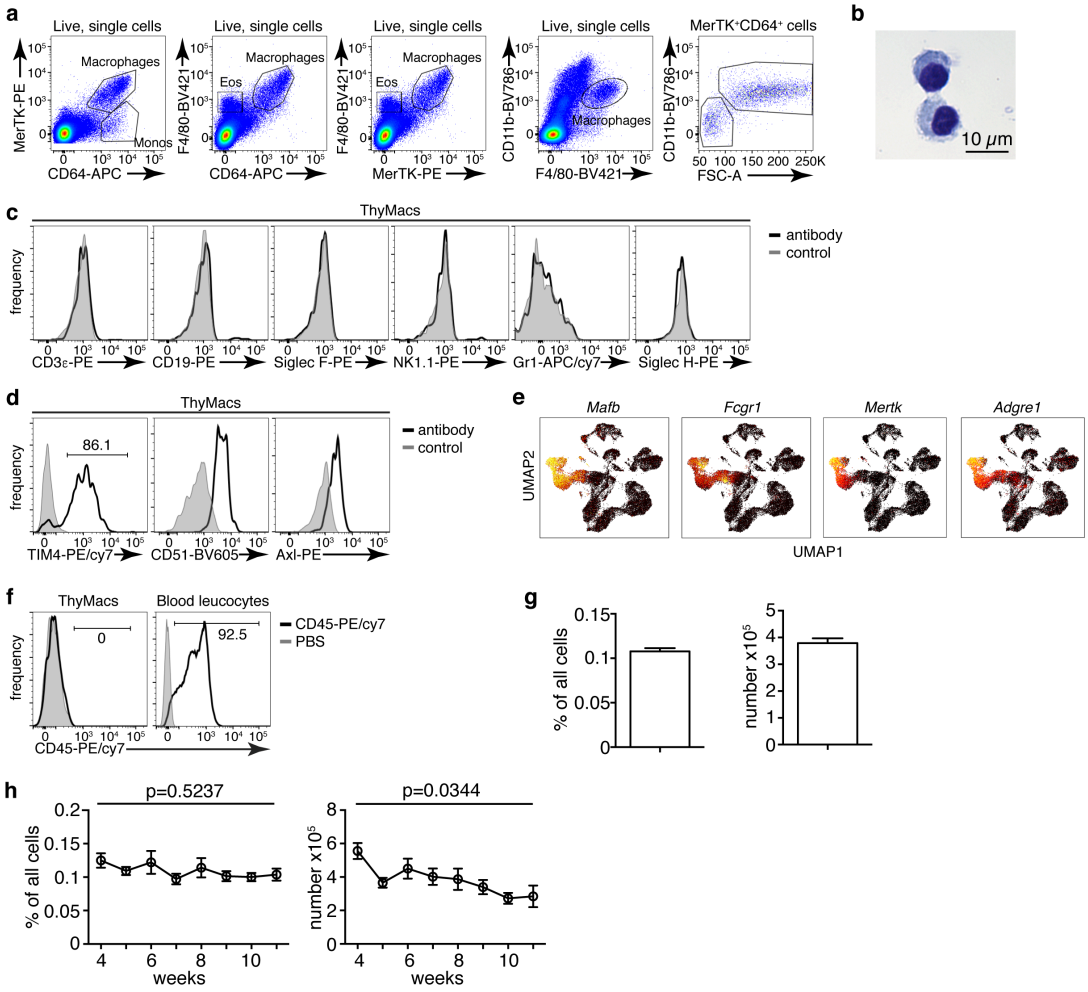

Figure 1. Thymic macrophages (ThyMacs) can be identified by the expression of CD64, MerTK and F4/80. a Flow cytometric analysis of enzymatically digested thymus tissue with macrophage markers CD64, MerTK, F4/80, and CD11b. More details about the confirmation of the identities of eosinophils and monocytes can be found in Fig. S1a and b. **b** Pappenheim (Hemacolor Rapid staining kit) staining of sorted ThyMacs. **c** Lack of expression of lineage markers associated with other cell types on ThyMacs. **d** The expression on ThyMacs of three receptors for phosphatidylserine that participate in the phagocytosis of apoptotic cells. **e** scRNA-Seq data showing the expression of prototypical macrophage genes *Mafb*, *Fcgr1* (CD64), *Mertk*, and *Adgre1* (F4/80) among thymus cells sorted

202 as *Csf1r*$^{GFP+}$ and *Cd11c*$^{YFP+}$. **f** Labeling of ThyMacs with intravenously
203 injected anti-CD45-PE antibody or PBS. The labeling of blood leucocytes is
204 shown for comparison. **g** Average numbers and percentages of ThyMacs in 4-
205 11 weeks old mice, n=82. **h** Comparison of the numbers and percentages of
206 ThyMacs in mice of different ages, n=82. All flow cytometry plots are
207 representative of at least 3 independent repeats. The numbers in the flow
208 cytometry plots are the percent of cells in the respective gates. Data in **g** and
209 **h** represent mean±SEM. Statistical significance in **h** was determined with one-
210 way ANOVA.

211

212 **Transcriptional signature of thymic macrophages**

213 To further understand the identity and functions of the thymic
214 macrophages, we sorted and subjected them to RNA sequencing analysis as
215 part of the IMMGEN's Open Source Mononuclear Phagocyte profiling.
216 Thymic macrophages displayed a transcription profile consistent with tissue-
217 resident macrophages and did not express genes characteristic of other
218 lineages (Fig. 2a). Then, we examined the expression of the core signature
219 macrophage genes[38] and found that they were enriched in thymic
220 macrophages but not in *Sirpa*$^{+}$ or *Xcr1*$^{+}$ thymic cDCs (Fig. 2b). On the
221 contrary, cDC core signature genes were abundantly expressed in both
222 thymic cDC subsets but not in thymic macrophages. These findings establish
223 that although thymic macrophages and cDCs share the thymic
224 microenvironment and expression of CD11c and MHC2, they have distinct
225 transcriptional profiles.

226 We then compared the gene expression profile of thymic macrophages to
227 that of other well-characterized macrophage populations available from
228 IMMGEN. Because of the abundance of samples, we limited our comparison
229 to only nine types of tissue-resident macrophages under steady-state
230 conditions – splenic red pulp macrophages, Kupffer cells, broncho-alveolar
231 lavage macrophages, large peritoneal cavity macrophages, white adipose
232 tissue macrophages, aorta macrophages, central nervous system microglia,
233 and spinal cord microglia. Hierarchical clustering revealed that thymic
234 macrophages were most closely related to splenic red pulp macrophages and
235 Kupffer cells (Fig. 2c).
236 To better identify the unique functions of thymic macrophages, we looked
237 for genes that were differentially expressed in these cells compared to other
238 tissue-resident macrophages. We set three criteria: 1) high expression in
239 thymic macrophages (>500); 2) >5 fold higher expression than the average
240 value in the nine populations of non-thymic macrophages; 3) expression in
241 thymic macrophages is higher than any non-thymic macrophage samples. A
242 total of 44 genes met these criteria, and we consider them to constitute the
243 transcriptional signature of thymic macrophages (Fig. 2d). These included
244 several degradation enzymes and their inhibitors (*Cst7*, *Mmp2*, *Mmp14*,
245 *Dnase1l3*, *Serpina3g*, *Acp5*), non-classical MHC molecules (*H2-M2*, *H2-Q6*,
246 *H2-Q7*), metabolic enzymes (*Chst2*, *Ass1*, *Kynu*, *Cp*, *Dgat2*, *Sorl1*, *Lap3*),
247 molecules involved in innate immunity (*Ifit2*, *Il18bp*, *Mefv*, *Lgals3bp*) and
248 extracellular signaling molecules and their receptors (*Pdgfa*, *Cxcl16*, *Il2rg*,
249 *Gpr157*). We also looked for transcription factors (TFs) highly expressed in
250 thymic macrophages and could potentially regulate critical gene networks in

251 these cells. A total of 25 TFs were highly expressed in thymic macrophages
252 (>250) and were at least 2-fold higher as compared to the non-thymic
253 macrophages (Table S1). Among them were several TFs involved in type I
254 interferon (IFN-I) signaling (*Stat1*, *Stat2*, *Irf7*, and *Irf8*) and lipid metabolism
255 (*Nr1h3*, *Pparg*, *Srebf1*, and *Rxra*) (Fig. 2e). Notably, *Runx3* that is important
256 for the development and function of cytotoxic T lymphocytes[48], innate
257 lymphoid cells[49], and Langerhans cells[50] was highly expressed in thymic
258 macrophages. *SpiC* that has well-documented roles in the development of red
259 pulp macrophages in the spleen, and bone marrow macrophages[51,52] was
260 also highly expressed in thymic macrophages, further strengthening the
261 argument for the similarity between thymus, spleen and liver macrophages.
262 To confirm the expression of *Spic* in thymic macrophages, we analyzed the
263 thymus of $Spic^{GFP}$ mice[52]. We found that all $Spic^{GFP+}$ cells were
264 macrophages (Fig. S4a and b), making them the most specific thymic
265 macrophage reporter strain compared with $Lyz2^{GFP}$, MAFIA ($Csf1r^{GFP}$),
266 $Cd11c^{YFP}$, and $Cx3cr1^{GFP}$ mice (Fig. S4c-e). However, only ~80% of thymic
267 macrophages were $Spic^{GFP+}$ suggesting heterogeneity within the cells (Fig.
268 S4f and g).
269 Several dominant pathways emerged when we grouped the 500 most
270 highly expressed genes in thymic macrophages according to gene ontology
271 (GO) terms (Fig. 2f). It was notable that five of the ten most highly enriched
272 GO pathways concerned antigen presentation of both exogenous and
273 endogenous antigens. These data complement our flow cytometry findings of
274 expression of MHC2 and suggest that thymic macrophages could be potent
275 antigen-presenting cells and might play a role in negative selection or agonist

selection of thymocytes. Two other highly enriched GO pathways were involved in lysosomal biogenesis and functions, highlighting the high capacity of these cells to degrade phagocytosed material. Thus, our transcriptional analysis has revealed that thymic macrophages are bona fide macrophages that bear significant similarity to spleen and liver macrophages and are specialized in lysosomal degradation of phagocytosed material and antigen presentation.

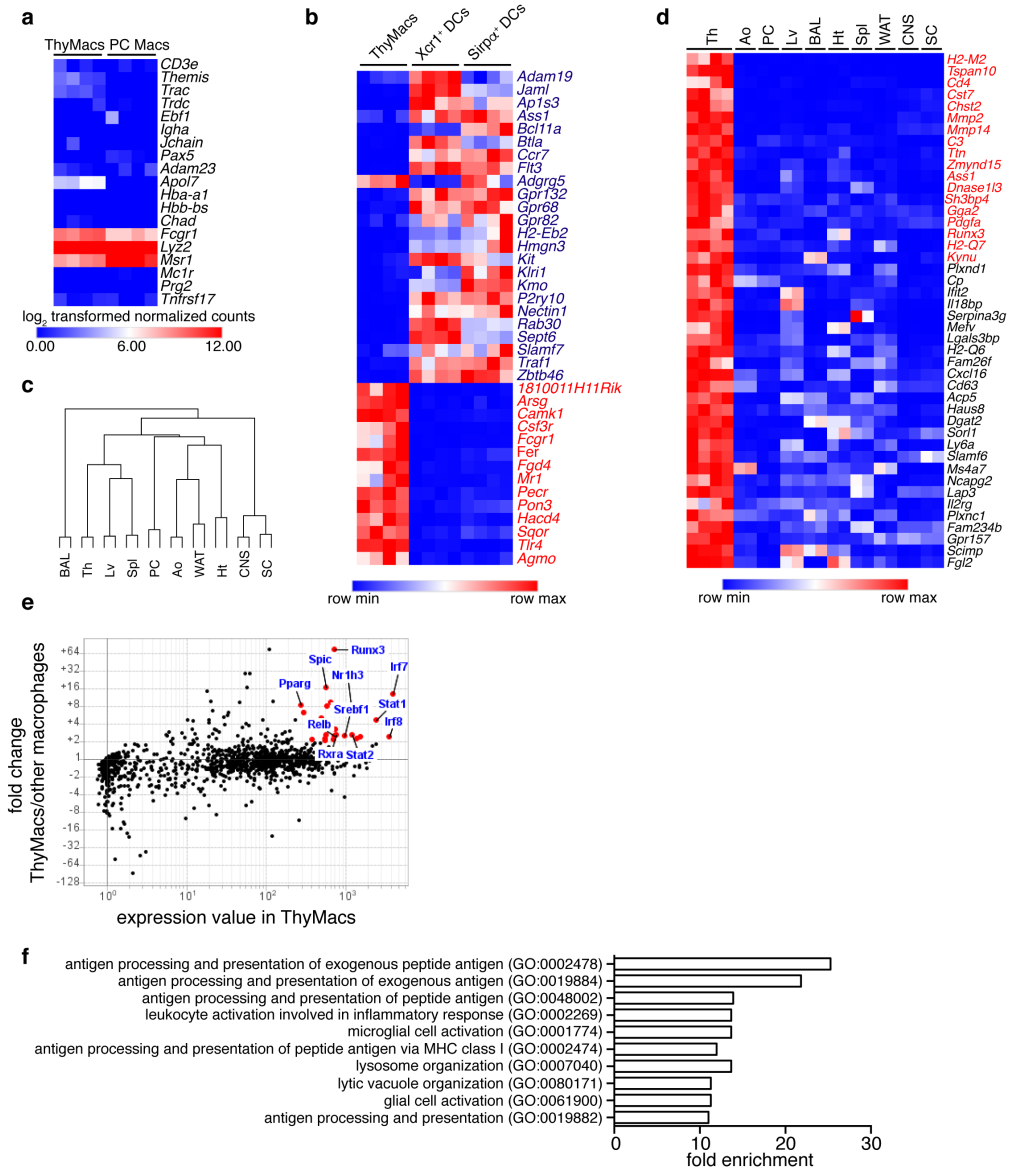

Figure 2. Transcriptional profile of thymic macrophages (ThyMacs). a Expression of lineage-specific genes in ThyMacs and peritoneal cavity macrophages (PC Macs). **b** Expression of cDC-specific genes (gene names in

286 blue) and macrophage-specific genes (gene names in red) in ThyMacs and
287 two populations of thymic cDCs (ThyDCs) – *Xcr1*$^{+}$ ThyDCs and *Sirpa*$^{+}$
288 ThyDCs. **c** Hierarchical clustering of ThyMacs and nine other populations of
289 tissue-resident macrophages in duplicates. **d** Highly expressed (>500) genes
290 enriched (>5-fold) in ThyMacs (4 samples) compared to nine other tissue-
291 resident macrophage populations (two samples each). The genes in red are
292 >10-fold up-regulated in thymic macrophages. **e** Comparison of the geometric
293 mean expression of transcription factors in thymic macrophages (4 samples)
294 and the nine other macrophage populations (2 samples each). Transcription
295 factors with expression >250 and fold change >2 are marked with red dots. **f**
296 Top 10 GO pathways in ThyMacs based on the 500 most highly expressed
297 genes in these cells. Th – ThyMacs, Spl – spleen red pulp macrophages, Lv –
298 Kupffer cells, BAL – bronchoalveolar lavage macrophages, PC – peritoneal
299 cavity macrophages, Ao – aorta macrophages, Ht – heart macrophages, WAT
300 – white adipose tissue macrophages, CNS – central nervous system
301 microglia, SC – spinal cord microglia.
302

303 **Yolk-sac progenitors contribute to embryonic thymic macrophages**

304 The ontogeny of thymic macrophages has been examined by only one
305 study since the realization that many tissue-resident macrophages are
306 descendants from embryonic progenitors[37]. Based on *Flt3*^{Cre} fate-mapping,
307 the authors concluded that most adult thymic macrophages derive from
308 HSCs. To determine if yolk-sac (YS) progenitors contribute to embryonic
309 thymic macrophages, we used *Cx3cr1*^{CreER} fate mapping[53]. Injection of 4-
310 OHT at E9.5 in *ROSA26*$^{LSL\text{-}GFP}$ mouse mated with a *Cx3cr1*^{CreER} male

311 permanently tags YS progenitors and their descendants with GFP (Fig. 3a).
312 Indeed, E19.5 microglia that are exclusively derived from YS progenitors were
313 labeled to a high degree (Fig. 3b). After adjusting for incomplete labeling
314 based on the microglia, we found that at E15.5 >50% of thymic macrophages
315 were fate mapped, i. e. from YS origin (Fig. 3c). However, GFP^+ thymic
316 macrophages decreased to just ~11% at E19.5, suggesting that YS
317 progenitors establish the embryonic thymic macrophage pool but are quickly
318 replaced by subsequent wave(s) of fetal liver monocytes or HSC-derived
319 macrophages.
320 To pinpoint when do the HSC-derived progenitors enter the thymus, we
321 devised two complementary experiments. First, we evaluated the contribution
322 of circulating adult monocytes to thymic macrophages without the
323 confounding effect of radiation damage on the thymus. We created shield
324 chimeras by subjecting CD45.1 mice to a lethal dose of irradiation while
325 protecting their upper body and the thymus with a 5 cm lead shield followed
326 by reconstitution with CD45.2 bone marrow (Fig. 3d). While the donor-derived
327 monocytes in the blood were, on average 20%, less than 2% of thymic
328 macrophages were $CD45.2^+$ (Fig. 3e and f), suggesting a relatively minor
329 (<10%) contribution of adult circulating monocytes to the thymic macrophage
330 pool consistent with a previous report[37]. Second, we transplanted E15.5
331 embryonic thymuses expressing GFP ubiquitously under the control of the
332 *ROSA26* locus (*ROSA26*^{GFP}) under the kidney capsule of adult mice and
333 analyzed them six weeks later (Fig. 3g). By that time, >99% of thymocytes
334 were derived from GFP^- host HSCs (Fig. 3h and i). As a positive control for
335 donor-derived cells, we used the thymic epithelial cells. The vast majority of

336 EpCAM⁺ thymic epithelial cells (>90%) were still GFP⁺. An identical
337 proportion of thymic macrophages was also GFP⁺. The results from our
338 transplantation experiments show that the progenitors of almost all thymic
339 macrophages are of embryonic origin. Altogether our results suggest that
340 resident thymic macrophages are derived from multiple waves of progenitors.
341 Initially, the thymus is settled by YS-derived progenitors that contribute
342 substantially to the thymic macrophage pool during the embryonic period. In
343 parallel with them, YS-independent progenitors infiltrate the thymus before
344 E15.5 and establish themselves as the dominant population before birth.
345 Adult HSC-derived monocytes contribute relatively little to the pool of thymic
346 resident macrophages in young adult mice.

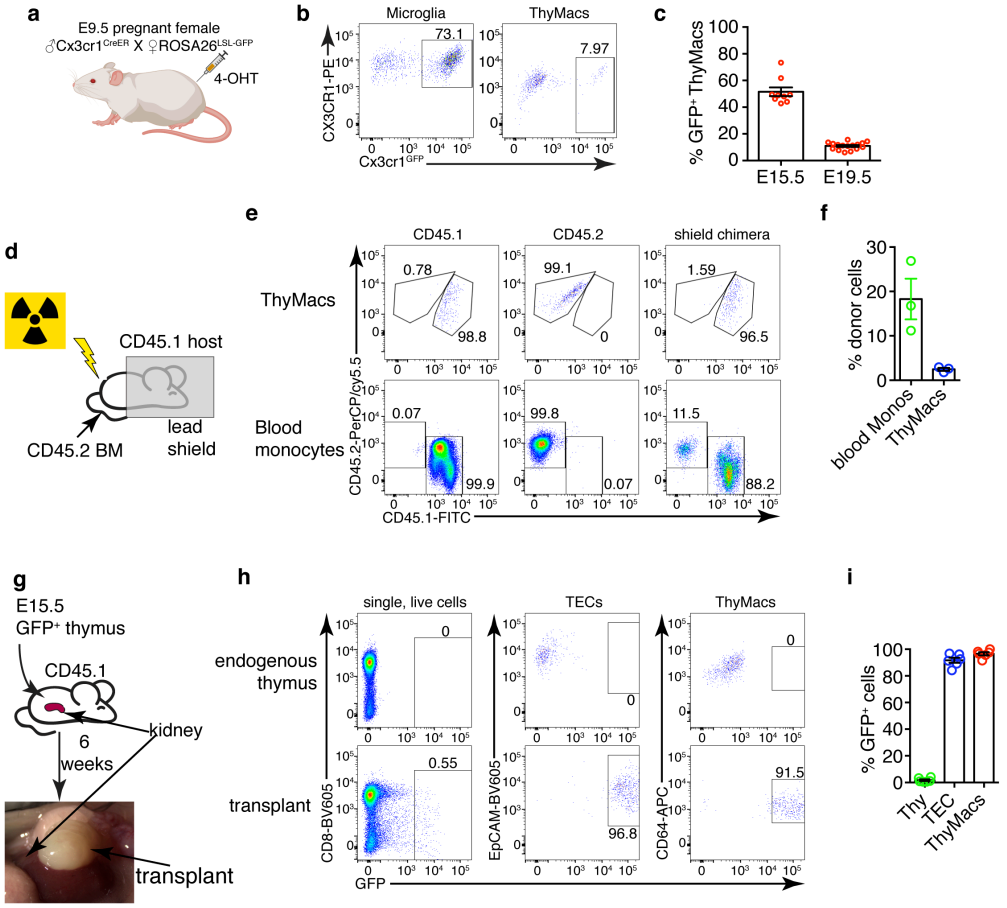

347 **Figure 3. Yolk sac (YS)-derived and non-YS-derived embryonic**
348 **progenitors sequentially contribute to the thymic macrophage pool. a**

349 Scheme of the YS-progenitor labeling experiments. E9.5 pregnant
350 *ROSA26*$^{LSL\text{-}GFP}$ mice mated with *Cx3cr1*^{CreER} males were injected with 4-
351 hydroxytamoxifen (4-OHT) and sacrificed at E15.5 or E19.5. **b** Representative
352 flow cytometry plots of the *Cx3cr1*^{GFP} expression in microglia (CD45^{+}CD11b^{+}
353 cells in the brain) and ThyMacs of the pups. **c** Frequencies of GFP^{+} ThyMacs
354 at E15.5 and E19.5 adjusted to the degree of labeling of microglia. **d** Scheme
355 of the shield chimera experiments. Congenic CD45.1 mice were lethally
356 irradiated with their upper body protected by a 5 cm thick lead shield and then
357 injected with CD45.2^{+} bone marrow. **e** Representative flow cytometric
358 analysis of ThyMacs and CD115^{+}CD11b^{+} blood monocytes for donor-derived
359 (CD45.2^{+}) cells. Non-chimeric CD45.1 and CD45.2 samples serve as controls
360 for the gating. **f** Frequencies of donor-derived ThyMacs and blood
361 monocytes. **g** Scheme of the thymus transplantation experiments. **h**
362 Representative flow cytometry plots of GFP expression in thymocytes (Thy),
363 CD45^{-}EpCAM^{+} thymic epithelial cells (TECs), and thymic macrophages
364 (ThyMacs) six weeks after the transplantation. The host thymus (endogenous
365 thymus) serves as a negative control. The percentages of GFP^{+} cells are
366 indicated in the plots. **i** Frequencies of GFP^{+} cells in different cell populations
367 in the transplanted thymus. Data in **c**, **f**, and **i** are mean±SEM with two litters,
368 three, and five mice per group, respectively. The numbers in the flow
369 cytometry plots are the percent of cells in the respective gates. Each dot is an
370 individual mouse or embryo.
371
372 **Thymic macrophages can proliferate in situ**

373 The fact that macrophages can persist for many weeks in the thymus
374 without constant replacement from blood monocytes suggests that they can
375 divide in situ. Staining for the proliferation marker Ki-67 revealed that ~4% of
376 the cells expressed this marker compared to an isotype control (Fig. 4a and
377 b). To obtain further proof that thymic macrophages are proliferative, we
378 tested the incorporation of the nucleotide analog 5-Ethynyl-2'-deoxyuridine
379 (EdU). Short-term EdU labeling experiments unexpectedly revealed that
380 thymic macrophages become EdU^+ with faster kinetics than thymocytes (Fig.
381 4c). The most likely explanation for this puzzling result is that some of the
382 thymic macrophages have engulfed apoptotic thymocytes that have recently
383 divided and incorporated EdU. Thus, EdU could have accumulated in these
384 macrophages through phagocytosis and not through cell division. To
385 circumvent this caveat, we designed a pulse-chase experiment (Fig. 4d).
386 Mice were injected daily with EdU for 21 days so that all cells that proliferate
387 in that period would incorporate the label. The vast majority of thymocytes
388 and thymic macrophages became EdU^+ at d. 21 (Fig. 4e). After 21 more days
389 of "chase period", only ~0.2% of thymocytes had retained the EdU label,
390 consistent with the existence of a very small population of long-term resident
391 thymocytes consisting mainly of regulatory T cells and NKT cells[54] (Fig. 4e
392 and f). However, ~5% of the thymic macrophages were EdU^+, suggesting
393 they divided during the labeling period. Finally, we sorted thymic
394 macrophages and subjected them to cell cycle analysis. Although almost all
395 thymic macrophages were in G0/G1 phase, a small population of ~3% was in
396 G2/M phase of the cell cycle (Fig. 4g and h). Collectively, three independent
397 approaches documented that 3-5% of thymic macrophages are actively

398 dividing under homeostatic conditions within the thymus. These findings can

399 explain the long-term maintenance of these cells within the organ without a

400 constant influx of progenitors.

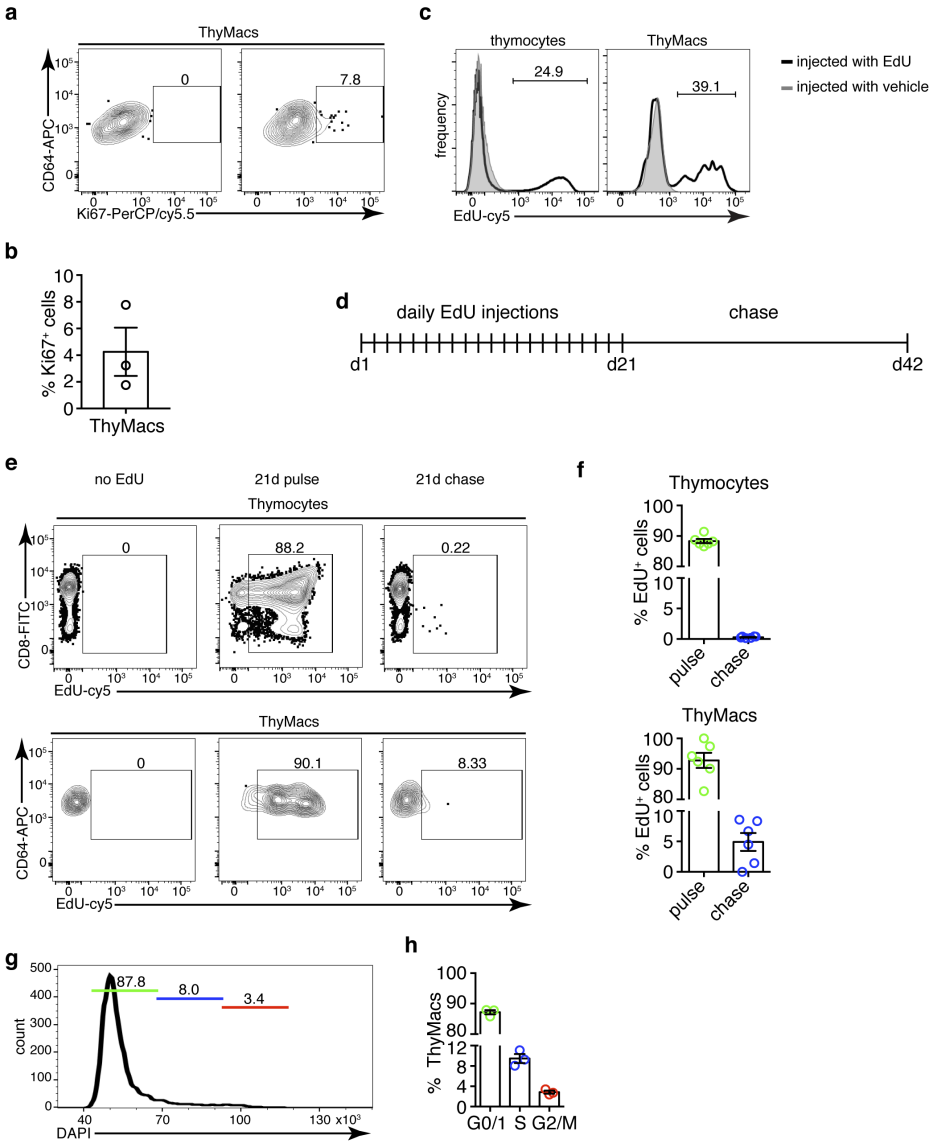

401 **Figure 4. Thymic macrophages exhibit a low degree of proliferation. a**

402 Example flow cytometry plots of Ki67 staining of thymic macrophages

403 (ThyMacs). **b** Frequency of Ki67^{+} thymic macrophages. **c** Example flow

404 cytometry plots of the EdU accumulation in thymocytes and thymic

405 macrophages 2 hours after 1 mg EdU i.p. or vehicle injection. The numbers

406 inside flow plots are the percentage of EdU^{+} cells from mice injected with

407 EdU. Data are representative of three independent experiments. **d** Scheme of
408 EdU pulse/chase experiment: mice were injected daily with 1 mg EdU i.p for
409 21 days and then rested for 21 more days. **e** Example flow cytometry plots of
410 EdU staining of thymocytes (upper row) and ThyMacs (lower row). **f**
411 Frequencies of EdU$^+$ cells among thymocytes (top graph) and ThyMacs
412 (bottom graph). **g** Example flow cytometry plot of cell cycle analysis of FACS
413 sorted ThyMacs. **h** Frequencies of ThyMacs in different stages of the cell
414 cycle. The numbers in the flow cytometry plots are the percent of cells in the
415 respective gates. Data are mean±SEM from three mice (**b** and **h**) or 6-7
416 individual mice (**f**). Each dot is an individual mouse.
417

418 **Expression of *Timd4* and *Cx3cr1 can distinguish* two populations of**
419 **thymic macrophages**

420 To determine if thymic macrophages are heterogeneous, we turned to our
421 scRNA-Seq data. Once we zoomed onto *Mafb* expressing cells, we could
422 distinguish three separate populations: 1) monocytes that expressed high
423 levels of *Ly6c2* and *Itgam* (CD11b) but did not express *Mertk*; 2) *Timd4*$^+$
424 (encoding TIM4) macrophages that also expressed high levels of *Spic* and
425 *Slc40a1*, but low levels of *Cx3cr1*; 3) *Cx3cr1*$^+$ macrophages that expressed
426 low levels of *Timd4*, *Spic*, and *Slc40a1* (Fig. 5a and b). Both macrophages
427 and monocytes expressed *Fcgr1* (CD64). A minority of macrophages
428 expressed high levels of *Mki67*, indicating that they might be proliferating,
429 corroborating our earlier data. Interestingly, most of the *Mki67* expressing
430 macrophages belonged to the *Cx3cr1*$^+$ population.

431 We confirmed the results from scRNA-Seq by flow cytometry. We could
432 identify discrete TIM4^{+}*Cx3cr1*$^{GFP-}$ and TIM4^{-}*Cx3cr1*$^{GFP+}$ macrophages (Fig.
433 5c). There was even TIM4^{+}*Cx3cr1*$^{GFP+}$ intermediate population that could not
434 be distinguished in the scRNA-Seq dataset, likely because of the lack of
435 statistical power. To determine the localization of the two distinct macrophage
436 populations, we stained thymic sections from *Cx3cr1*^{GFP} mice with an antibody
437 to MerTK. The *Cx3cr1*$^{GFP-}$ MerTK^{+} cells correspond to *Timd4*$^{+}$ macrophages,
438 while the *Cx3cr1*$^{GFP+}$MerTK^{+} cells would be the *Cx3cr1*$^{GFP+}$ macrophages.
439 Strikingly, the two macrophage populations showed distinct localization.
440 *Timd4*$^{+}$ macrophages were located in the cortex, while the *Cx3cr1*$^{GFP+}$
441 macrophages resided in the medulla and the cortico-medullary junction (Fig.
442 5d).
443 To better understand the differences between the two populations of thymic
444 macrophages, we looked for differentially expressed genes. We included the
445 thymic monocytes in the comparison, as these cells clustered the closest to
446 macrophages. *Timd4*$^{+}$ macrophages expressed the highest levels of the
447 transcription factors *Spic*, *Maf*, and *Nr1h3*; the receptors for apoptotic cells
448 *Axl*, *Mertk*, and *Timd4*; and many Slc transporters such as *Slc40a1*, *Slc1a3*,
449 *Slco2b1*, *Slc11a1*, and *Slc7a7* (Fig. 5e and Table S2). *Cx3cr1*$^{+}$ macrophages
450 expressed high levels of the transcription factor *Runx3*; a distinct set of
451 phosphatidylserine receptors such as *Stab1*, *Anxa5*, and *Anxa3*; many
452 degradative enzymes such as *Mmp2*, *Mmp14*, *Dnase1l3*, *Acp5*, *Lyz2*, *Ctsz*,
453 *Ctss*, *Ctsd*, *Ctsl*; cytokines such as *Pdgfa*, *Cxcl16*, and *Ccl12*; and molecules
454 involved in MHC1 antigen presentation such as *B2m*, *H2-M2*, *H2-K1*, *H2-Q7*.
455 Thymic monocytes were characterized by differential expression of the typical

456 monocyte genes *Ly6c2*, *Ccr2*, and *S100a4*, and genes involved in MHC2

457 antigen presentation such as *Ciita*, *H2-DMb1*, *H2-Ab1*, and *Cd74*.

458

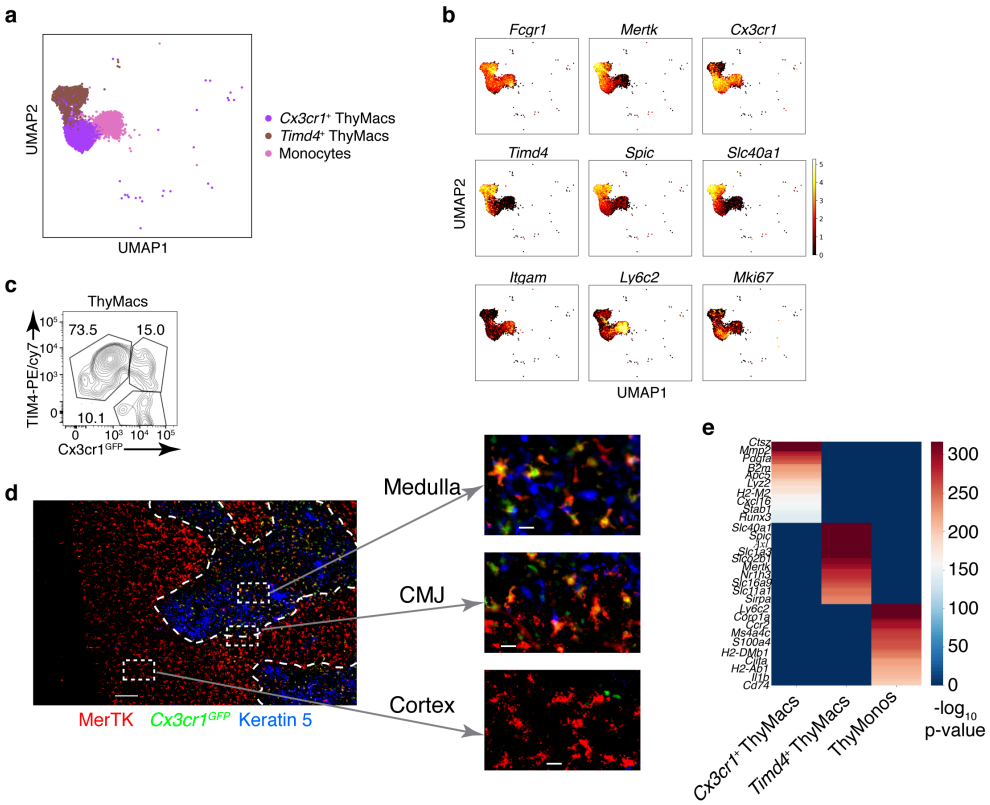

459 Figure 5: **Two populations of macrophages with distinct localization**

460 **exist in the thymus. a** UMAP clusters from Fig. S2 with high expression of

461 the transcription factor *Mafb* fall into three groups: monocytes, *Timd4*$^{+}$

462 macrophages, and *Cx3cr1*$^{+}$ macrophages. **b** Expression of the indicated

463 genes in the three *Mafb*-positive clusters. **c** A flow cytometry plot of *Cx3cr1*^{GFP}

464 and TIM4 expression in ThyMacs. The plot is representative of >10 individual

465 experiments. The numbers inside the plot are the percentages of the cell

466 populations in the respective gates. **d** Immunofluorescent staining of the

467 thymus of *Cx3cr1*^{GFP} mouse stained with MerTK (a marker for all

468 macrophages) and Keratin 5 (a marker for medulla). The scale bar is 150 μm.

469 Areas in the cortex, medulla, and the cortico-medullary junction (CMJ)

470 represented by the dashed boxes are enlarged below to show the co-

471 localization of *Cx3cr11*^{GFP} and MerTK signal in CMJ and medulla, but not in
472 cortex. The scale bars in the images below are 20 μm. The images are
473 representative of three individual mice. **e** Differentially expressed genes
474 among *Timd4*$^{+}$ thymic macrophages, *Cx3cr1*$^{+}$ thymic macrophages, and
475 thymic monocytes. The negative $\log_{10}$ p-values for the genes expressed in
476 each cluster were calculated as described in the Materials and Methods, and
477 the top 50 differentially expressed genes were plotted in the figure. Ten of
478 these genes are listed on the left.
479

480 ***Cx3cr1*$^{+}$ cells give rise to *Timd4*$^{+}$ cells during embryonic development**

481 To determine if the two populations of thymic macrophages are related, we
482 first analyzed the kinetics of their appearance during embryonic development.
483 At the earliest time point (E14.5), all thymic macrophages were *Cx3cr1*$^{+}$, and
484 only ~20% of them were also TIM4^{+} (Fig. 6a and b). The proportion of TIM4^{+}
485 cells increased at E17.5, and TIM4^{+}*Cx3cr1*$^{-}$ cells started to appear. In the
486 neonatal period, almost all macrophages were TIM4^{+}, and very few remained
487 TIM4^{-}. The proportion of TIM4^{-} cells increased in 6 weeks old mice, but TIM4^{+}
488 macrophages remained the dominant population. These kinetics (Fig. 6c) are
489 consistent with *Timd4*$^{+}$ macrophages developing from *Cx3cr1*$^{+}$ cells before
490 birth. Another plausible scenario is that distinct progenitors give rise to
491 different thymic macrophages populations (e.g., YS-progenitors give rise to
492 *Cx3cr1*$^{+}$*Timd4*$^{-}$ and HSC-derived progenitors develop into *Timd4*$^{+}$
493 macrophages). To test the latter hypothesis, we re-visited the fate mapping of
494 YS progenitors results (Fig. 3a). Although a larger part (~60% at E15.5) of
495 *Cx3cr1*$^{+}$TIM4^{-} cells were derived from YS progenitors (Fig. 6d), a substantial

496 proportion (~40% at E15.5) of YS-derived TIM4$^+$ macrophages could clearly
497 be identified at both E15.5 and E19.5, suggesting that YS progenitors can
498 give rise to both *Cx3cr1*$^+$ and *Timd4*$^+$ cells. Extrapolating from the data, the
499 non-YS-derived progenitors (GFP$^-$ cells) can also give rise to both *Timd4*$^-$ and
500 *Timd4*$^+$ cells. Thus, the simplest explanation for our findings is that *Timd4*$^+$
501 cells develop from *Cx3cr1*$^+$ cells during embryonic development. This
502 transition is complete in the first week after birth as there were essentially no
503 *Cx3cr1*$^+$ thymic macrophages remaining at d.7 (Fig. 6a and b).

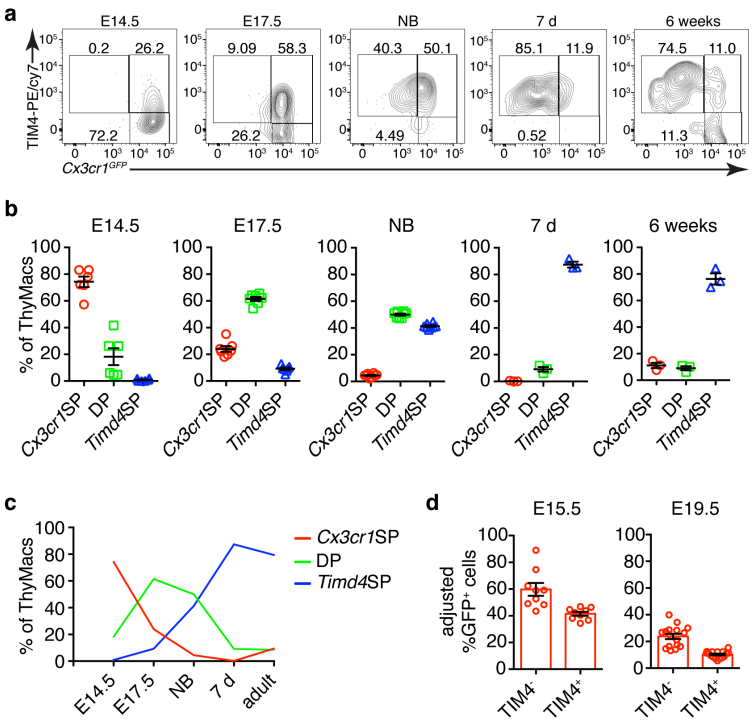

504

505 **Figure 6. *Timd4*$^+$ thymic macrophages are derived from *Cx3cr1*$^+$ cells**
506 **during embryonic development. a** Example flow cytometry plots for the
507 expression of *Cx3cr1*^{GFP} and TIM4 on thymic macrophages at different times
508 during embryonic development (E14.5, E17.5), immediately after birth, at 7
509 days, and 6 weeks of age. **b** Frequencies of *Timd4*$^+$*Cx3cr1*$^-$ (*Timd4* single-
510 positive or *Timd4*SP), *Timd4*$^+$*Cx3cr1*$^+$(double-positive or DP), and
511 *Cx3cr1*$^+$*Timd4*$^-$ (*Cx3cr1* single-positive or *Cx3cr1*SP) thymic macrophages at

512 the indicated time points. **c** Kinetics of the changes in different subpopulations
513 of thymic macrophages from E14.5 to 6 weeks. **d** Frequencies at E15.5 and
514 E19.5 of GFP-labeled cells among *TIM4*$^{+}$ or *TIM4*$^{-}$ cells in *Cx3cr1*^{CreER} X
515 *ROSA26*$^{LSL\text{-}GFP}$ embryos treated with 4-OHT at E9.5. Data is from at least two
516 independent experiments for each panel. Each symbol is an individual mouse
517 or embryo.
518
519 ***Timd4*$^{+}$ thymic macrophages self-maintain, while *Cx3cr1*$^{+}$ cells slowly**
520 **accumulate with age**
521 To understand how are the resident thymic macrophage populations
522 maintained during adult life, we induced recombination in *Cx3cr1*^{CreER} X
523 *ROSA26*$^{LSL\text{-}GFP}$ mice during the neonatal period (Fig. 7a) or at 6 weeks of age
524 (Fig. 7c) and compared the proportion of GFP^{+} cells 3 and 42 days after
525 labeling. The extent of labeling of *Timd4*$^{+}$ thymic macrophages did not
526 change within these 6 weeks, no matter whether the mice were treated with
527 Tamoxifen in the first week after birth or at 6 weeks (Fig. 7b and d),
528 suggesting steady-state maintenance and absence of a significant influx from
529 unlabeled cells (e.g., monocytes). In contrast, the proportion of labeled
530 *Timd4*$^{-}$ thymic macrophages decreased significantly 6 weeks after Tamoxifen
531 injection in both neonatal and adult mice, suggesting that this population was
532 being diluted by unlabeled cells. To further substantiate these findings, we
533 examined older WT mice and found out that the proportions of *Timd4*$^{-}$ thymic
534 macrophages increased with age, and in mice >8 months old, they accounted
535 for ~70% of all macrophages in the organ (Fig. 7e). Thus, we conclude that
536 *Timd4*$^{+}$ macrophages can maintain themselves for long periods in the cortex

537 of the thymus, Since the first week of life, *Cx3cr1*⁺ cells are slowly being

538 recruited to the medulla and cortico-medullary junction, and in aging mice

539 form the predominant phagocytic population in the organ.

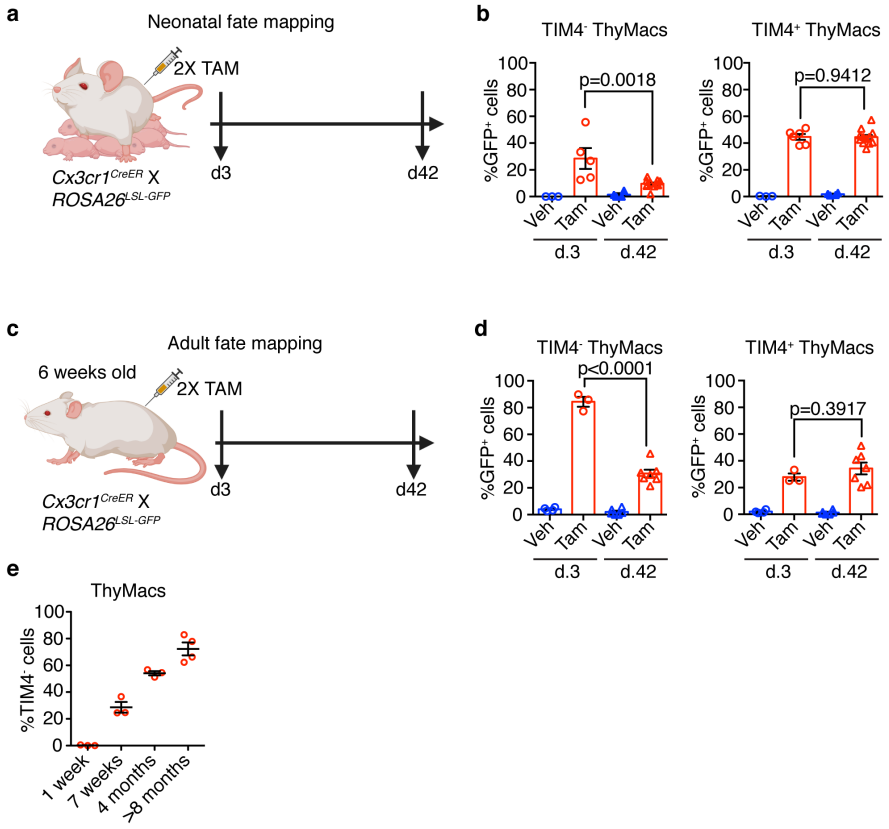

540

541 **Figure 7. *Timd4*⁺ thymic macrophages self-maintain during adult life,**

542 **while *Cx3cr1*⁺ cells slowly accumulate with age. a** Scheme of the neonatal

543 fate mapping: A nursing dam was injected twice with Tamoxifen (Tam) or

544 vehicle (Veh) in the first week after giving birth to *Cx3cr1*^{CreER} X *ROSA26*$^{LSL-}$

545 ^{GFP} pups. Three or 42 days after the last injection, the pups were sacrificed,

546 and the degree of labeling of *Timd4*⁺ and *Timd4*⁻ thymic macrophages was

547 examined by flow cytometry. **b** Frequencies of GFP⁺ *Timd4*⁺ or *Timd4*⁻ thymic

548 macrophages from neonatally fate mapped mice after 3 and 42 days. Vehicle

549 injected nursing dam litters (Veh) served as a control for non-specific labeling.

550 **c** Scheme of the adult fate mapping: Six weeks old *Cx3cr1*^{CreER} X *ROSA26*$^{LSL-}$

551 ^{GFP} mice were injected twice with Tamoxifen (Tam) or vehicle (Veh). Three or

552 42 days after the last injection, the mice were sacrificed, and the degree of
553 labeling of *Timd4*$^{+}$ and *Timd4*$^{-}$ thymic macrophages was examined by flow
554 cytometry. **d** Frequencies of GFP^{+} *Timd4*$^{+}$ or *Timd4*$^{-}$ thymic macrophages
555 from adult fate mapped mice after 3 and 42 days. **e** Frequencies of TIM4^{-}
556 thymic macrophages at different ages. The data is mean±SEM from 2
557 independent experiments (**b**) or at least 3 individual mice per time point (**d** and
558 **e**). Each symbol is an individual mouse. Statistical significance was
559 determined with unpaired Student's t-test.
560

561 **Discussion**

562 Here, we have described the phenotype, transcriptional profile, localization,
563 diversity, ontogeny, and maintenance of macrophages in the thymus. These
564 cells express the typical macrophage markers CD64, MerTK, and F4/80 and
565 are transcriptionally most similar to splenic red pulp macrophages and liver
566 Kupffer cells. However, they have a unique expression profile dominated by
567 genes involved in antigen presentation and lysosomal degradation. We found
568 that thymic macrophages consist of two populations with distinct localization.
569 *Timd4*$^{+}$ macrophages occupied the cortex, while *Cx3cr1*$^{+}$ cells were located in
570 the medulla and the cortico-medullary junction. While YS-derived
571 macrophages dominated the early stages of thymus development, they were
572 quickly replaced by non-YS embryonic progenitors that gave rise to the
573 *Timd4*$^{+}$ thymic macrophages that could proliferate and self-maintain. *Cx3cr1*$^{+}$
574 macrophages started slowly accumulating after birth and in old mice became
575 the most abundant population.

576 Altogether our data depict thymic macrophages as typical tissue-resident
577 macrophages with origin from multiple hematopoietic waves, ability to self-
578 maintain, and expression of the core macrophage-specific genes. They were
579 most similar transcriptionally to splenic red pulp macrophages and Kupffer
580 cells, which is not surprising considering that they all specialize in
581 efferocytosis and have efficient lysosomal degradation machinery. These
582 three populations also shared expression of the transcription factor *Spic* that
583 is induced by heme released following red blood cells phagocytosis[52].
584 However, the thymus is not known as a place for erythrocyte degradation.
585 Thus the mechanism for *Spic* up-regulation in thymic macrophages is unclear.
586 The unique features of thymic macrophages include high expression of
587 genes involved in the IFN-I pathway, antigen presentation, and lysosomal
588 degradation. The up-regulation of IFN-I-stimulated genes such as *Stat1*,
589 *Stat2*, *Irf7*, and *Irf8* can be explained by the constitutive secretion of IFN-I by
590 thymic epithelial cells[55,56]. The purpose of IFN-I expression in the thymus
591 in the absence of a viral infection is unclear. Still one possibility is that it
592 mediates negative selection to IFN-dependent genes as part of central
593 tolerance.
594 Thymic macrophages highly express molecules involved in antigen
595 presentation, including MHC1 and MHC2, although the latter is expressed at
596 lower levels than in cDCs. Thus, they have the potential to present antigens
597 for both negative selection and agonist selection. These two activities have
598 traditionally been assigned solely to cDCs[57]. However, recent evidence
599 suggests that negative selection is most efficient when the cell that presents
600 the antigen to auto-reactive thymocytes is also the one that phagocytoses

601 it[58]. So, macrophages participation in thymocyte selection needs to be re-
602 evaluated with optimized isolation procedures and specific genetic tools.
603 The extraordinary ability of thymic macrophages to engulf and degrade
604 apoptotic thymocytes has been appreciated for a long time[31], and our RNA-
605 Seq data provides additional supporting evidence for this function by
606 highlighting the up-regulation of pathways involved in lysosomal degradation.
607 An interesting topic for future research would be to understand how the
608 metabolites derived from apoptotic cells are returned to the microenvironment
609 to support the proliferation of immature thymocytes. A *SoLute Carrier* (*Slc*)
610 genes-based program has been described in vitro[59], but its relevance to
611 tissue-resident macrophages remains to be determined. Altogether, our study
612 demonstrates that thymic macrophages are a unique subset of tissue-resident
613 macrophages and support the idea that resident macrophage phenotype is
614 determined by the combination of ontogeny, microenvironment, and other
615 factors[60].
616 Together with the study by Tacke et al., our work builds the following model
617 for thymic macrophage origin[37]: Thymic macrophages develop in three
618 distinct waves: YS-derived progenitors dominate the early stages of thymus
619 development but are replaced before birth by a second wave of YS-
620 independent embryonic progenitors that forms the bulk of thymic
621 macrophages after birth and can self-maintain into adulthood. With age, there
622 is a slow and steady influx of *Timd4*$^{-}$*Cx3cr1*$^{+}$ macrophage precursors that
623 occupy the medulla and cortico-medullary junction, becoming the major
624 phagocytic population in the thymus of older mice (>8 months). The second
625 wave of YS-independent macrophages is most likely the progeny of

626 embryonic HSCs based on *Flt3*^{Cre} fate mapping that showed that >80% of
627 thymic macrophages in adult mice are descendants of HSCs[37]. Whether
628 HSC-independent fetal liver monocytes contribute to thymic macrophages and
629 to what extend awaits the creation of models that can specifically target this
630 population of progenitors. Recruitment of circulating monocytes to the resident
631 macrophage pool in the thymus has been ruled out previously by parabiosis
632 and *Ccr2*$^{-/-}$ mice[37]. Our shield chimera experiments have arrived at similar
633 conclusions. However, the relatively short duration of these experiments and
634 their focus on the bulk thymic macrophages have prevented the recognition of
635 the gradual accumulation of *Timd4*$^{-}$ macrophages. Once we zoomed in on this
636 minor cell population in young mice, the fate mapping clearly showed an influx
637 of unlabeled progenitors. Whether the progenitors of *Timd4*$^{-}$ macrophages
638 are monocytes remains to be formally demonstrated. However, in all
639 macrophage populations exhibiting replacement in adults examined to date,
640 monocytes have been singled out as the source[12,19,22,24,25,30]. An
641 alternative possibility involves thymocyte progenitors that under certain
642 circumstances have been shown to differentiate into macrophages and
643 granulocytes in the thymus[42,43]. However, if this occurs in unmanipulated
644 mice at a steady-state remains unclear.
645 The strict spatial segregation of the two macrophage populations in the
646 thymus implies that they might have distinct functions. *Timd4*$^{+}$ cells are
647 restricted to the cortex and are particularly abundant in the deeper cortex,
648 close to the medulla. Both positive and negative selection of thymocytes occur
649 there, so we speculate that *Timd4*$^{+}$ macrophages might be specialized in
650 efferocytosis of CD4^{+}CD8^{+} (double-positive) thymocytes that cannot interact

651 with cortical thymic epithelial cells and die by neglect or are auto-reactive and
652 undergo clonal deletion in the cortex[61]. On the other hand, *Cx3cr1*$^+$
653 macrophages accumulate in the medulla; the thymic region specialized in
654 negative selection to tissue-restricted antigens (TRA). They might contribute
655 to the process in several ways: 1) by carrying TRAs from blood and peripheral
656 organs. A similar process has been described for cDC2 (SIRPα^+ DCs)[62]. In
657 fact, *Cx3cr1*$^+$ thymic macrophages could have contributed to this role because
658 they were not distinguished from cDC2 in this study. 2) By capturing TRAs
659 from *Aire*$^+$ medullary thymic epithelial cells and presenting them to auto-
660 reactive thymocytes as shown for DCs[63-65]. 3) By phagocytosing apoptotic
661 TRA-specific medullary thymocytes, a process we have observed before[58].
662 The exact involvement of thymic macrophages in the selection events in the
663 thymus remains to be determined.
664 The accumulation of the *Cx3cr1*$^+$ cells in older mice has clear implications
665 for thymus aging. One key feature of thymus involution is the accumulation of
666 extracellular matrix produced by fibroblasts and the emergence of white
667 adipocytes[66]. The *Cx3cr1*$^+$ subset is the predominant producer of the growth
668 factor PDGFα that is required for the maintenance of adipocyte stem cells and
669 can stimulate tissue fibrosis[67,68]. The gradual accumulation of *Cx3cr1*$^+$
670 macrophages could increase the availability PDGFα in the aging thymus
671 stimulating extracellular matrix production and differentiation of precursors
672 into adipocytes. This model predicts that limiting the influx of *Cx3cr1*$^+$
673 macrophage precursors could delay thymus involution.
674 Recent work described a novel phagocytic and antigen-presenting cell type
675 in the thymus called monocyte-derived DCs[65]. The phenotype of these cells

676 overlaps with the CD64^{+}F4/80^{lo}CD11b^{+} cells in our study. However, we favor
677 the classification of these cells as monocytes based on their expression of
678 *Mafb*, CD64, and Ly6C (Fig. 5b) and lack of expression of the defining DC
679 transcription factor *Zbtb46* (Fig. S2c)[69]. As monocytes can differentiate into
680 cDC2, particularly in the context of inflammation[70], the precise identity and
681 the relationship of this population to thymic cDC2 remain to be established.
682 In the past several years, scRNA-Seq has come to the forefront of
683 biologists' efforts to disentangle the cellular diversity of tissues. Several
684 comprehensive studies have included samples from mouse or human
685 thymus[71-73]. However, in these studies, too few thymic macrophages were
686 sampled to give meaningful clustering results. Efforts specifically targeting
687 the thymus have provided considerably more information[74,75], but
688 macrophage diversity was still not recognized. Characterization of rare
689 populations such as thymic macrophages (~0.1% of all cells in the thymus)
690 requires optimized enzymatic digestion procedures and enrichment strategies,
691 as has been demonstrated already for thymic epithelial cells[76,77]. Our
692 scRNA-Seq dataset provides a rich resource for the unbiased characterization
693 of myeloid cells in the thymus and will greatly aid in the understanding of the
694 myeloid landscape of the thymus.
695 In summary, our work comprehensively characterizes macrophages in the
696 thymus and paves the way for exploration of their functions.
697
698 **Materials and methods**
699 **Mice**

700 C57BL/6Narl (CD45.2) mice were purchased from the National Laboratory
701 Animal Center, Taipei, Taiwan. MAFIA (MAcrophage Fas-Induced Apoptosis)
702 [78], *Cx3cr1*^{GFP} [79], *Spic*^{GFP} [52], *Cx3cr1*^{CreER} [53], and *B6.SJL-Ptprca*
703 *Pepcb/BoyJ* (CD45.1) mice were purchased from the Jackson Laboratories.
704 *Cd11c*^{YFP} [80] and *Lyz2*^{GFP} [81] mice have been described. Mice ubiquitously
705 expressing GFP from the *ROSA26* locus were generated by breeding
706 *Pdgfra*^{Cre} [82] and *ROSA26*$^{LSL\text{-}ZsGreen}$ (also known as *ROSA26*$^{LSL\text{-}GFP}$ or Ai6)
707 mice[83] (both from the Jackson Laboratories). A mouse from this cross was
708 identified, in which the STOP cassette was deleted in the germline. It was
709 designated *ROSA26*^{GFP} and subsequently bred to C57BL/6 mice. All mice
710 were used at 4-10 weeks of age unless otherwise specified. Mice were bred
711 and maintained under specific pathogen-free conditions at the animal facility
712 of National Yang-Ming University. All experimental procedures were approved
713 by the Institutional Animal Care and Use Committee (IACUC) of National
714 Yang-Ming University.
715
716 **Treatment with 5-Ethynyl-2'-deoxyuridine (EdU)**
717 Mice were i.p. injected with 1 mg EdU (Carbosynth) dissolved in PBS daily
718 for 21 days and then rested for 21 more days. Cells from the thymus were
719 harvested on day 21 or 42. In some experiments, the mice were sacrificed 2
720 hours after the first EdU injection.
721
722 **Shield chimera generation**
723 CD45.1 mice were anesthetized by i.p. injection of 120 μg/g body weight
724 Ketamine hydrochloride (Toronto Research Chemicals) and 12 μg/g body

725 weight Xylazine hydrochloride (Sigma). Anesthetized mice were taped to a 5
726 cm thick lead block so that the lead block covered the head and the chest
727 down to the bottom of the rib cage. Then, they were irradiated with a lethal
728 dose (1000 rad) from a ^{137}Cs source (Minishot II, AXR) so that only their
729 abdomen and hind legs were exposed. After recovery from anesthesia, the
730 mice were transfused i.v. with 10^7 bone marrow cells from a congenic
731 (CD45.2) donor. Then, they were given Trimerin (0.5 mg/mL Sulfadiazine +
732 0.1 mg/mL Trimethoprim, China Chemical and Pharmaceutical Co., Tainan,
733 Taiwan) in the drinking water for the first two weeks after the irradiation and
734 analyzed after six weeks.
735
736 **Cell isolation from thymus, blood, and peritoneal cavity**
737 Thymocytes were obtained by mechanical disruption of the thymus with a
738 syringe plunger. For myeloid cell isolation, mouse thymuses were cut into
739 small pieces and digested with 0.2 mg/mL DNase I (Roche) and 0.2 mg/mL
740 collagenase P (Roche) in complete DMEM for 20 min at 37˚C with frequent
741 agitation. 1.6 mg/mL Dispase I (ThermoFisher) was added to the enzymatic
742 mixture for thymic epithelial cell isolation. In some experiments, thymic
743 myeloid cells and thymic epithelial cells were enriched by 57% Percoll PLUS
744 (GE Healthcare) discontinuous gradient centrifugation at 4˚C, 1800 rpm, for
745 20 min without brake. Cells at the interface were collected and washed with
746 PBS to remove residual silica particles. Then the cells were resuspended in
747 PBS with 0.5% BSA (HM Biological), filtered through a 70 μm filter, and kept
748 on ice.
749

750 Blood was isolated by cardiac puncture of sacrificed mice and immediately
751 diluted with PBS. After centrifugation, the cell suspensions were treated with
752 ammonium chloride-potassium lysis buffer for 3 min on ice once or twice.
753 Peritoneal cavity cells were obtained by lavage with 5 mL PBS + 2 mM EDTA
754 (Merck). Following gentle massage, the cavity was opened with an abdominal
755 incision, and lavage fluid was collected.
756
757 **Flow cytometry**
758 Single-cell suspensions (0.5 – 2X10^6 cells) from thymus, blood, or
759 peritoneal cavity were blocked with supernatant from 2.4G2 hybridoma (a kind
760 gift by Dr. Fang Liao, Academia Sinica, Taipei, Taiwan) and stained with
761 fluorochrome- or biotin-labeled antibodies for 20 min on ice in PBS + 0.5%
762 BSA + 2 mM EDTA + 0.1% NaN_3 (FACS buffer). The following antibodies
763 were used: CD11b (clone M1/70), MHC2 (M5/114.15.2), CD11c (N418),
764 F4/80 (BM8), CD115 (AFS98), SIRPα (P84), CD45 (30-F11), NK1.1 (PK136),
765 TIM4 (RMT4-54), Gr-1 (RB6-8C5), CD64 (X54-5/7.1), Siglec H (551), Ly6C
766 (HK1.4), CD3ε (145-2C11), CD8α (53-6.7), CD19 (6D5), B220 (RA3-6B2),
767 CD4 (GK1.5), CD51 (RMV-7), CD45.1 (A20), CD45.2 (104), CX3CR1
768 (SA011F11), and EpCAM (G8.8) from BioLegend; Axl (MAXL8DS), MerTK
769 (DS5MMER), and Ki67 (SolA15) were from eBioscience; Siglec F (E50-2440),
770 CD90.2 (30-H12), and CD11c (HL3) were from BD Biosciences. Cells were
771 washed, and if necessary, incubated for 20 more min with fluorochrome-
772 labeled Streptavidin: Streptavidin-AF647 (Jackson Immunoresearch) or
773 Streptavidin-APC/cy7, Streptavidin-BV421, Streptavidin-BV605 (BioLegend).
774 After the last wash, the cells were resuspended in FACS buffer containing

775 DAPI (BioLegend), Propidium Iodide (Sigma), or DRAQ7 (BioLegend) and
776 analyzed immediately on an LSR Fortessa flow cytometer running Diva 8
777 software (BD Biosciences). Typically, 500,000 cells were collected from
778 thymus samples. Data were analyzed using FlowJo software (TreeStar).
779
780 For intracellular staining, after surface antibody staining, the cells were
781 labeled with Zombie Aqua (BioLegend) for 30 min in ice. Then, the cells were
782 fixed with 2% paraformaldehyde (Electron Microscope Sciences) in PBS for
783 20 min on ice, permeabilized with either 0.5% Triton-X 100 (Sigma) for 20 min
784 on ice, or with Foxp3 staining kit (eBioscience) according to the protocol
785 provided by the manufacturer, and stained with antibodies for intracellular
786 markers for 40-60 min on ice.
787
788 For cell cycle analysis, 1-5X10^5 sorted thymic macrophages were fixed with
789 70% ethanol for 2 h on ice. The cells were spun down at 1800 rpm for 20 min
790 at 4˚C, washed with PBS, and stained with 1 μg/ml DAPI (BioLegend) for 30
791 min at room temperature in the dark.
792
793 For EdU staining, after surface marker and Zombie Aqua staining, cells
794 were fixed with 2% paraformaldehyde in PBS for 20 min on ice and
795 permeabilized with 0.5% Triton X-100 in PBS at room temperature for 20 min.
796 EdU was detected by adding an equal volume of 2X Click reaction buffer
797 consisting of 200 mM Tris, 200 mM ascorbic acid (Acros), 8 mM $CuSO_4$
798 (Acros), 8 μM Cy5-azide (Lumiprobe) to the permeabilized cells resuspended
799 in 0.5% Triton X-100 in PBS and incubation at room temperature for 30 min.

800 Cells were washed twice with 0.5% Triton X-100 in PBS and analyzed on a
801 flow cytometer.
802
803 **Cell sorting**
804 The sorting of thymic macrophages was done following the IMMGEN
805 guidelines. Briefly, the thymuses of 3 male C57BL/6Narl mice were harvested
806 in ice-cold staining buffer containing phenol red-free DMEM (Gibco) with 10
807 mM HEPES (Sigma), 0.1% NaN_3, and 2% FBS (Gibco). Single-cell
808 suspensions were prepared as described in the Flow cytometry section.
809 Percoll PLUS was used to enrich mononuclear cells. The cells were
810 resuspended at 10^8/mL in staining buffer and labeled with appropriate
811 antibodies for 15 min in ice. To sort thymic macrophages, the cells were first
812 labeled with biotinylated antibodies to lineage markers (Lin) – CD3, CD8, Gr1,
813 B220. After washing, the cells were stained with antibodies to CD11b, F4/80,
814 CD45, CD64, and Streptavidin-APC/cy7 for 15 min in ice. For sorting thymus
815 $XCR1^+$ and $SIRP\alpha^+$ cDCs, antibodies to XCR1, SIRPα, CD11c, MHC2, CD64,
816 and F4/80 were used. For sorting peritoneal cavity macrophages, antibodies
817 to ICAM2 and F4/80 were used. Immediately before sorting, the dead cells
818 were excluded with DRAQ7 or PI. For RNA Sequencing experiments, the
819 cells were double-sorted on FACS Melody, or Aria cell sorters (BD
820 Biosciences) and 1000 cells were directly deposited in TCL buffer (Qiagen),
821 frozen in dry ice and sent to IMMGEN for RNA sequencing. Four biological
822 replicates were prepared. For cytospin and cell cycle analysis, 1-5X10^5 cells
823 sorted on FACS Melody were collected in staining buffer.
824

825 **Cytospin**

826 Sorted cells were mounted on Superfrost PLUS slides (Thermo Scientific)
827 using a Cytospin centrifuge (Cytospin 3, Shandon) for 5 min at 500 rpm. Cells
828 were fixed with 2% paraformaldehyde for 10 min at room temperature and
829 stained with the Hemacolor Rapid Staining Kit (Merck Millipore). Images were
830 collected on BX61 upright microscope (Olympus) using 100X objective with
831 immersion oil and captured with a CCD camera. Images were then analyzed
832 and processed with ImageJ (NIH) and Adobe Photoshop 5.5 (Adobe).

833

834 **RNA sequencing analysis**

835 RNA sequencing was done at IMMGEN using Smart-seq2 protocol[84,85]
836 on a NextSeq500 sequencer (Illumina). Following sequencing, raw reads
837 were aligned with STAR to the mouse genome assembly mm10 and assigned
838 to specific genes using the GENCODE vM12 annotation. Gene expression
839 was normalized by DESeq2[86] and visualized by Morpheus
840 (https://software.broadinstitute.org/morpheus). Hierarchical clustering was
841 done with Cluster 3.0 and visualized with Java TreeView. Only genes with
842 SD>20 were used (10602 genes). The metric used was Pearson correlation
843 (uncentered), and the clustering method was average linking. Gene
844 expression of mouse transcription factors[87] was visualized in MultiplotStudio
845 of GenePattern[88]. GO enrichment was calculated and visualized in R by
846 using clusterProfiler[89].

847

848 **Timed pregnancies and embryonic thymus analysis**

849 To set up timed pregnancies, each male mouse (*Cx3cr1*$^{CreER/CreER}$,
850 *Cx3cr1*$^{GFP/GFP}$ or C57BL/6) and female mouse (*ROSA26*$^{LSL\text{-}GFP/LSL\text{-}GFP}$ or
851 C57BL/6) were housed together in the same cage for one night and separated
852 on the next day, which we defined as embryonic day 0.5 (E0.5). Female mice
853 were assumed to be pregnant if their weight gain was over 2 g at E8.5[90].
854 Thymuses from E14.5 and E17.5 embryos, neonatal, 1-weeks-old pups, and
855 adult mice (older than 6-weeks-old) were harvested, mechanically dissociated
856 with plastic sticks in 1.5-mL centrifuge tubes, and enzymatically digested with
857 0.2 mg/mL DNase I and 0.2 mg/mL collagenase P in complete DMEM for 20
858 min at 37˚C with frequent agitation. The cells were resuspended in PBS with
859 0.5% BSA, filtered through a 70 μm filter, kept on ice, and used flow
860 cytometric analysis as described in the Flow Cytometry section.
861
862 **Genetic fate mapping – E9.5, neonatal and adult**
863 For genetic fate mapping, timed pregnancies of *Cx3cr1*$^{CreER/CreER}$ male and
864 *ROSA26*$^{LSL\text{-}GFP/LSL\text{-}GFP}$ female mice were set up as described. To label the
865 *Cx3cr1*$^{+}$ erythromyeloid progenitors derived from embryonic yolk sac[8], 4-
866 hydroxytamoxifen (4-OHT from Sigma) was administered i.p. to pregnant
867 females on E9.5 at a dose of 75 μg/g (body weight). To improve the survival
868 of embryos and reduce the risk of abortions, Progesterone (Sigma) was co-
869 injected at a dose of 37.5 μg/g (body weight)[91]. To label the *Cx3cr1*$^{+}$ thymic
870 macrophages in *Cx3cr1*^{CreER} X *ROSA26*$^{LSL\text{-}GFP}$ neonates and adult mice,
871 Tamoxifen (TAM from Sigma) was injected i.p. at a dose of 2 mg/mouse to
872 lactating dams on postnatal day 3 and 4 (P3 and P4) or to adult mice for 2

873 consecutive days. Thymuses were harvested and analyzed 3 days or 6
874 weeks after the last injection by flow cytometry.
875
876 **scRNA-Seq – sorting, library generation, and sequencing**
877 scRNA-Seq was performed at the Genomics Center for Clinical and
878 Biotechnological Applications of NCFB (NYCU, Taipei, Taiwan). Briefly, the
879 thymuses of one female MAFIA and 2 male *Cd11c*^{YFP} mice were harvested
880 and enzymatically digested as described previously. Mononuclear cells were
881 enriched by 57% Percoll PLUS discontinuous centrifugation, washed to
882 remove silica particles, and resuspended at 10^6/mL in PBS with 0.04% BSA.
883 The cell suspensions were filtered through Falcon 35 μm strainer (Corning)
884 and stained with viability dye (PI or DAPI) immediately before sorting. Cell
885 sorting was performed on a FACS Melody sorter (BD Biosciences) running
886 FACS Chorus (BD Biosciences) software in purity mode. $3X10^5$ GFP or YFP
887 positive cells under the live/singlet gating were collected into 5 ml round
888 bottom tubes pre-coated with 0.04% BSA in PBS. Sorted cells were washed
889 and resuspended in 300 μL PBS with 0.04% BSA and then filtered again into
890 1.5-mL DNA LoBind tubes (Eppendorf) through a 35 μm strainer. The viability
891 of the cells was evaluated by Countess II (Invitrogen) and Trypan Blue
892 (ThermoFisher), and samples with cell viability rates higher than 85% were
893 used for encapsulation and library preparation. Single-cell encapsulation and
894 library preparation were performed using Single Cell 3' v3/v3.1 Gene
895 Expression solution (10x Genomics). All the libraries were processed
896 according to the manufacturer's instruction and sequenced on NovaSeq 6000
897 (Illumina) platform at the NHRI (Zhubei, Taiwan). Post-processing and quality

898 control were performed by the NYCU Genome Center using the CellRanger
899 package (v. 3.0.2, 10x Genomics). Reads were aligned to mm10 reference
900 assembly. Primary assessment with CellRanger reported 9,973 cell-barcodes
901 with 11,385 median unique molecular identifiers (UMIs, transcripts) per cell
902 and 3,076 median genes per cell sequenced to 71.0% sequencing saturation
903 with 94,260 mean reads per cell for MAFIA mouse sample; 9,801 cell-
904 barcodes with 13,467 median UMIs per cell and 3,211 median genes per cell
905 sequenced to 74.9% sequencing saturation with 119,820 mean reads per cell
906 for the first *Cd11c*^{YFP} mouse sample; 12,938 cell-barcodes with 14,439
907 median UMIs per cell and 3,199 median genes per cell sequenced to 71.4%
908 sequencing saturation with 108,585 mean reads per cell for the second
909 *Cd11c*^{YFP} mouse sample.
910
911 **Analysis of scRNA-Seq**
912 Preprocessing
913 The Scanpy[92] pipeline was used to read the count matrix. Three batches
914 of samples (one from GFP^{+} cells from MAFIA mouse and two from YFP^{+} cells
915 from *Cd11c*^{YFP} mice) were preprocessed independently and integrated later.
916 Cells that expressed <200 genes and genes that were expressed in <3 cells
917 were filtered out. The percentage of mitochondrial genes was calculated -and
918 cells with >10% mitochondrial genes were removed. Cells with >7,000 genes
919 or <1,000 genes were also removed. Read counts were normalized to library
920 size 10,000 and log-transformed with scanpy.pp.log1p function.
921 Datasets integration and batch effect correction

922 Read count matrices and spliced/unspliced matrices were merged first.
923 Principal Component Analysis was applied to reduce dimensions to 70.
924 BBKNN[93] was then used to remove batch effects with the
925 scanpy.external.pp.bbknn function with default parameters.
926 Visualization and clustering
927 UMAP[94] provided by scanpy was used to visualize data with default
928 parameters. K-nearest neighbor and Leiden clustering were applied
929 sequentially to cluster cells into groups. K-nearest neighbor graph
930 construction was done by scanpy.pp.neighbors with parameters
931 n_neighbors=12 and n_pcs=70. Leiden clustering was then performed by
932 scanpy.tl.leiden with parameter resolution=0.15. To improve UMAP
933 visualization, scanpy.tl.paga was applied, and we trimmed unnecessary graph
934 edges by scanpy.tl.paga with threshold=0.018.
935 Marker genes and statistics
936 Wilcoxon rank-sum tests were applied to examine differentially expressed
937 genes. Clusters were selected from the result of Leiden clustering.
938 Differentially expressed genes of a cluster against other clusters were
939 identified by scanpy.tl.rank_genes_groups and scanpy.pl.rank_genes_groups.
940 P-values were collected for each cluster and transformed by negative $\log_{10}$ for
941 better visualization. The top 50 differentially expressed genes were visualized
942 in the figure.
943
944 **Immunofluorescent staining**
945 Dissected thymus lobes from C57BL/6 mice were cleaned of connective
946 tissue and fixed in 4% paraformaldehyde (Sigma) for 1 h at 4˚C, washed in

947 PBS, submerged in 10% sucrose, and then in 30% sucrose for 12 h each.
948 The tissue was then frozen in Tissue-Tek OCT compound (Sakura Fintek) for
949 cryostat sectioning. 10 or 20 μm thick sections were prepared with CryoStar
950 NX50 (ThermoFisher) on Superfrost PLUS (ThermoScientific) microscope
951 slides, dried overnight, and stored at -80˚C until used. Before staining, the
952 sections were fixed with acetone (Sigma) at -20˚C for 10 min, air-dried, then
953 blocked with 5% goat serum + 5% donkey serum (both from Jackson
954 Immunoresearch) in PBS for 2 h and stained with primary antibodies: rat
955 monoclonal to MerTK (DS5MMER, eBioscience), rat monoclonal to TIM4
956 (RMT4-54, Bio-X-Cell) or rabbit polyclonal to Keratin 5 (BioLegend) overnight
957 at 4˚C in a humidified chamber. After washing in PBS, the sections were
958 labeled with goat anti-rat-Alexa Fluor 647 (Invitrogen) or goat anti-rat Cy3
959 (Jackson Immunoresearch) and donkey anti-rabbit AF647 (Jackson
960 Immunoresearch) secondary antibodies for 2 hours at room temperature,
961 followed by 5 min staining with DAPI. TUNEL Assay was done with the Click-
962 iT Plus TUNEL Assay Alexa Fluor 647 kit (Invitrogen) according to the
963 manufacturer's recommendations. A positive (pre-incubation with DNase I for
964 30 min at room temperature) and negative (no TdT enzyme) controls were
965 always included. The sections were mounted with 0.1% n-propyl gallate
966 (Sigma) in glycerol (Sigma) and imaged with an AxioObserver 7 (Carl Zeiss)
967 wide-field microscope equipped with Plan Apochromat 20x NA=0.8 objective
968 (Zeiss) and AxioCam 702 mono camera (Zeiss) and controlled by Zen 2.3
969 Blue (Zeiss) software. Image analysis was performed with Imaris 8.0.2
970 (Bitplane).
971

972 The co-localization scoring for MerTK and TIM4 with TUNEL was done with
973 Imaris 8.2 (Bitplane). TUNEL$^+$ cells were detected with the Spots function,
974 while MerTK$^+$ and TIM4$^+$ cells were detected with the Surface function. Spots
975 that co-localize with Surfaces were identified with the “Find Spots close to
976 Surface” function of Imaris XT. The threshold for co-localization was set to 5
977 µm. The results were manually curated so that Spots categorized as “not co-
978 localized” that were: 1) at the edge of the imaging field were excluded from
979 consideration; 2) with clear Surface signal around them were re-categorized
980 as "co-localized". The ratio of co-localized Spots to all Spots was calculated
981 and presented as the co-localization index.
982
983 **Thymus transplantation**
984 To obtain E15.5 embryos, *ROSA26^{GFP}* homozygous male and C57BL/6
985 female mice were mated in a cage overnight and separated on the next day.
986 Pregnant mice were sacrificed 15 days later, the viable embryos were
987 harvested, and the thymuses were isolated in ice-cold PBS. C57BL/6
988 recipients were anesthetized by i.p injection of Ketamine hydrochloride (120
989 µg/g, Toronto Research Chemicals) and Xylazine hydrochloride (12 µg/g,
990 Sigma). The fur on the left flank was removed, and the left kidney was
991 exposed by cutting the skin, muscle layer, and peritoneum. The kidney
992 capsule was nicked with a G23 needle, and the fetal thymus was pushed into
993 the pocket under the kidney capsule with a G23 needle equipped with a
994 plunger from a spinal needle. After the kidney was re-positioned back into the
995 peritoneal cavity, the peritoneum was sutured, and the skin was stapled with
996 metal clips. Rymadil (Carprofen, 5 µg/g, Zoetis) was given subcutaneously to

997 ease the wound pain, and Trimerin (Sulfadiazine at 0.5 mg/mL + Trimethoprim
998 at 0.1 mg/mL) were given in the drinking water for the first two weeks after the
999 surgery. The metal clips were removed from the skin after the first week, and
1000 the transplanted thymus and recipient's endogenous thymus were harvested
1001 and analyzed six weeks after the kidney transplantation.
1002
1003 **Statistical analysis**
1004 Comparison between groups was made with Prism 6 (GraphPad Software).
1005 Comparisons between two groups were carried out with unpaired Student's t-
1006 test. When more than two groups were compared, a one-way ANOVA with
1007 Tukey correction was used. Differences were considered significant if $p<0.05$.
1008
1009 **Data availability**
1010 The RNA Sequencing data of thymic macrophages and thymic dendritic
1011 cells is available at NCBI Gene Expression Omnibus (GEO) as part of
1012 GSE122108 and at www.immgen.org. The single cell RNA sequencing data is
1013 deposited at NCBI GEO under accession number. The source data
1014 underlying Fig. 1g-h, Fig. 3c, f, i, Fig. 4b. f, h, Fig. 6b, d, Fig. 7b, d, e, Fig.
1015 S1h, Fig. S3c, and Fig. S4b, d, e, g are provided in the Source Data files. All
1016 other data supporting the findings of this study are available within the article
1017 and its figures and tables.
1018
1019 **Abbreviations:**
1020 cDC – classical dendritic cell
1021 DC – dendritic cell

1022 EdU – 5-Ethynyl-2'-deoxyuridine

1023 GO – gene ontology

1024 HSC – hematopoietic stem cell

1025 IFN-I – type I Interferon

1026 IMMGEN – Immunological Genome Consortium

1027 scRNA-Seq – single-cell RNA sequencing

1028 TF – transcription factor

1029 ThyMacs – thymic macrophages

1030 TRA – tissue-restricted antigen

1031 YS – yolk sac

1032 **References:**

1033 1. Wynn TA, Chawla A, Pollard JW. Macrophage biology in development,
1034 homeostasis and disease. Nature. Nature Publishing Group; 2013;496:
1035 445–455. doi:10.1038/nature12034

1036 2. Baratin M, Simon L, Jorquera A, Ghigo C, Dembele D, Nowak J, et al. T
1037 Cell Zone Resident Macrophages Silently Dispose of Apoptotic Cells in
1038 the Lymph Node. Immunity. Elsevier Inc; 2017;47: 349–362.e5.
1039 doi:10.1016/j.immuni.2017.07.019

1040 3. A-Gonzalez N, Castrillo A. Origin and Specialization of Splenic
1041 Macrophages. Cellular Immunology. 2018;330: 1–27.
1042 doi:10.1016/j.cellimm.2018.05.005

1043 4. Bellomo A, Mondor I, Spinelli L, Lagueyrie M, Stewart BJ, Brouilly N, et
1044 al. Reticular Fibroblasts Expressing the Transcription Factor WT1
1045 Define a Stromal Niche that Maintains and Replenishes Splenic Red
1046 Pulp Macrophages. Immunity. Elsevier Inc; 2020;53: 127–142.e7.
1047 doi:10.1016/j.immuni.2020.06.008

1048 5. van Furth R, Cohn ZA. The origin and kinetics of mononuclear
1049 phagocytes. J Exp Med. Rockefeller University Press; 1968;128: 415–
1050 435. doi:10.1084/jem.128.3.415

1051 6. Ginhoux F, Guilliams M. Tissue-Resident Macrophage Ontogeny and
1052 Homeostasis. Immunity. 2016;44: 439–449.
1053 doi:10.1016/j.immuni.2016.02.024

1054 7. Perdiguero EG, Klapproth K, Schulz C, Busch K, Azzoni E, Crozet L, et
1055 al. Tissue-resident macrophages originate from yolk-sac-derived
1056 erythro-myeloid progenitors. Nat Immunol. Nature Publishing Group;
1057 2015;518: 547–551. doi:10.1038/nature13989

1058 8. Mass E, Ballesteros I, Farlik M, Halbritter F, Günther P, Crozet L, et al.
1059 Specification of tissue-resident macrophages during organogenesis.
1060 Science. American Association for the Advancement of Science;
1061 2016;353: aaf4238–aaf4238. doi:10.1126/science.aaf4238

1062 9. Ginhoux F, Greter M, Leboeuf M, Nandi S, See P, Gokhan S, et al. Fate
1063 mapping analysis reveals that adult microglia derive from primitive
1064 macrophages. Science. 2010;330: 841–845.
1065 doi:10.1126/science.1194637

1066 10. Hoeffel G, Wang Y, Greter M, See P, Teo P, Malleret B, et al. Adult
1067 Langerhans cells derive predominantly from embryonic fetal liver
1068 monocytes with a minor contribution of yolk sac–derived macrophages.
1069 J Exp Med. 2012;209: 1167–1181. doi:10.1084/jem.20120340

1070 11. Hoeffel G, Chen J, Lavin Y, Low D, Almeida FF, See P, et al. C-Myb(+)
1071 erythro-myeloid progenitor-derived fetal monocytes give rise to adult
1072 tissue-resident macrophages. Immunity. 2015;42: 665–678.
1073 doi:10.1016/j.immuni.2015.03.011

1074 12. Goldmann T, Wieghofer P, Jordão MJC, Prutek F, Hagemeyer N,
1075 Frenzel K, et al. Origin, fate and dynamics of macrophages at central
1076 nervous system interfaces. Nat Immunol. 2016;17: 797–805.
1077 doi:10.1038/ni.3423

1078 13. Hashimoto D, Chow A, Noizat C, Teo P, Beasley MB, Leboeuf M, et al.
1079 Tissue-Resident Macrophages Self-Maintain Locally throughout Adult
1080 Life with Minimal Contribution from Circulating Monocytes. Immunity.
1081 Elsevier Inc; 2013;38: 792–804. doi:10.1016/j.immuni.2013.04.004

1082 14. Epelman S, Lavine KJ, Beaudin AE, Sojka DK, Carrero JA, Calderon B,
1083 et al. Embryonic and Adult-Derived Resident Cardiac Macrophages Are
1084 Maintained through Distinct Mechanisms at Steady State and during
1085 Inflammation. Immunity. Elsevier Inc; 2014;40: 91–104.
1086 doi:10.1016/j.immuni.2013.11.019

1087 15. Sheng J, Ruedl C, Karjalainen K. Most Tissue-Resident Macrophages
1088 Except Microglia Are Derived from Fetal Hematopoietic Stem Cells.
1089 Immunity. Elsevier Inc; 2015;43: 382–393.
1090 doi:10.1016/j.immuni.2015.07.016

1091 16. Liu Z, Gu Y, Chakarov S, Bleriot C, Kwok I, Chen X, et al. Fate Mapping
1092 via Ms4a3-Expression History Traces Monocyte-Derived Cells. Cell.
1093 Elsevier; 2019;178: 1509–1525.e19. doi:10.1016/j.cell.2019.08.009

1094 17. Ensan S, Li A, Besla R, Degousee N, Cosme J, Roufaiel M, et al. Self-

1095 renewing resident arterial macrophages arise from embryonic
1096 CX3CR1+ precursors and circulating monocytes immediately after birth.
1097 Nat Immunol. Nature Publishing Group; 2015;17: 159–168.
1098 doi:10.1038/ni.3343

1099 18. Mondor I, Baratin M, Lagueyrie M, Saro L, Henri S, Gentek R, et al.
1100 Lymphatic Endothelial Cells Are Essential Components of the
1101 Subcapsular Sinus Macrophage Niche. Immunity. Elsevier Inc; 2019;50:
1102 1453–1466.e4. doi:10.1016/j.immuni.2019.04.002

1103 19. Molawi K, Wolf Y, Kandalla PK, Favret J, Hagemeyer N, Frenzel K, et
1104 al. Progressive replacement of embryo-derived cardiac macrophages
1105 with age. J Exp Med. 2014;211: 2151–2158. doi:10.1084/jem.20140639

1106 20. Heidt T, Courties G, Dutta P, Sager HB, Sebas M, Iwamoto Y, et al.
1107 Differential Contribution of Monocytes to Heart Macrophages in Steady-
1108 State and After Myocardial Infarction. Circulation Research. 2014;115:
1109 284–295. doi:10.1161/CIRCRESAHA.115.303567

1110 21. Yahara Y, Barrientos T, Tang YJ, Puviindran V, Nadesan P, Zhang H,
1111 et al. Erythromyeloid progenitors give rise to a population of osteoclasts
1112 that contribute to bone homeostasis and repair. Nat Cell Biol. Springer
1113 US; 2020;22: 1–28. doi:10.1038/s41556-019-0437-8

1114 22. Jacome-Galarza CE, Percin GI, Muller JT, Mass E, Lazarov T, Eitler J,
1115 et al. Developmental origin, functional maintenance and genetic rescue
1116 of osteoclasts. Nature. Nature Publishing Group; 2019;568: 541–545.
1117 doi:10.1038/s41586-019-1105-7

1118 23. Calderon B, Carrero JA, Ferris ST, Sojka DK, Moore L, Epelman S, et
1119 al. The pancreas anatomy conditions the origin and properties of
1120 resident macrophages. J Exp Med. 2015;212: 1497–1512.
1121 doi:10.1084/jem.20150496

1122 24. Tamoutounour S, Guilliams M, Sanchis FM, Liu H, Terhorst D, Malosse
1123 C, et al. Origins and Functional Specialization of Macrophages and of
1124 Conventional and Monocyte-Derived Dendritic Cells in Mouse Skin.
1125 Immunity. Elsevier Inc; 2013;39: 925–938.
1126 doi:10.1016/j.immuni.2013.10.004

1127 25. Bain CC, Bravo-Blas A, Scott CL, Gomez Perdiguero E, Geissmann F,
1128 Henri S, et al. Constant replenishment from circulating monocytes
1129 maintains the macrophage pool in the intestine of adult mice. Nat
1130 Immunol. 2014;15: 929–937. doi:10.1038/ni.2967

1131 26. Sierro F, Evrard M, Rizzetto S, Melino M, Mitchell AJ, Florido M, et al. A
1132 Liver Capsular Network of Monocyte-Derived Macrophages Restricts
1133 Hepatic Dissemination of Intraperitoneal Bacteria by Neutrophil
1134 Recruitment. Immunity. Elsevier Inc; 2017;47: 374–388.e6.
1135 doi:10.1016/j.immuni.2017.07.018

1136 27. Mossadegh-Keller N, Gentek R, Gimenez G, Bigot S, Mailfert S,
1137 Sieweke MH. Developmental origin and maintenance of distinct
1138 testicular macrophage populations. J Exp Med. 2017;214: 2829–2841.
1139 doi:10.1084/jem.20170829

1140 28. Lokka E, Lintukorpi L, Cisneros-Montalvo S, Mäkelä J-A, Tyystjärvi S,
1141 Ojasalo V, et al. Generation, localization and functions of macrophages
1142 during the development of testis. Nature Communications. Springer US;
1143 2020;11: 1–16. doi:10.1038/s41467-020-18206-0

1144 29. Wang M, Yang Y, Cansever D, Wang Y, Kantores C, Messiaen S, et al.
1145 Two populations of self-maintaining monocyte-independent
1146 macrophages exist in adult epididymis and testis. PNAS. 2020;118:
1147 e2013686117. doi:10.1073/pnas.2013686117/-/DCSupplemental

1148 30. Bain CC, Hawley CA, Garner H, Scott CL, Schridde A, Steers NJ, et al.
1149 Long-lived self-renewing bone marrow-derived macrophages displace
1150 embryo-derived cells to inhabit adult serous cavities. Nature
1151 Communications. Nature Publishing Group; 2016;7: 1–14.
1152 doi:10.1038/ncomms11852

1153 31. Surh CD, Sprent J. T-cell apoptosis detected in situ during positive and
1154 negative selection in the thymus. Nature. 1994;372: 100–103.
1155 doi:10.1038/372100a0

1156 32. Esashi E, Sekiguchi T, Ito H, Koyasu S, Miyajima A. Cutting Edge: A
1157 possible role for CD4+ thymic macrophages as professional scavengers
1158 of apoptotic thymocytes. Journal of Immunology (Baltimore, Md : 1950).
1159 American Association of Immunologists; 2003;171: 2773–2777.
1160 doi:10.4049/jimmunol.171.6.2773

1161 33. Liu L-T, Lang Z-F, Li Y, Zhu Y-J, Zhang J-T, Guo S-F, et al.
1162 Composition and characteristics of distinct macrophage subpopulations
1163 in the mouse thymus. Molecular Medicine Reports. 2013;7: 1850–1854.
1164 doi:10.3892/mmr.2013.1448

1165 34. Guerri L, Peguillet I, Geraldo Y, Nabti S, Premel V, Lantz O. Analysis of
1166 APC types involved in CD4 tolerance and regulatory T cell generation
1167 using reaggregated thymic organ cultures. J Immunol. American
1168 Association of Immunologists; 2013;190: 2102–2110.
1169 doi:10.4049/jimmunol.1202883

1170 35. Lopes N, Charaix J, Cédile O, Sergé A, Irla M. Lymphotoxin alpha fine-
1171 tunes T cell clonal deletion by regulating thymic entry of antigen-
1172 presenting cells. Nature Communications. Springer US; 2018;9: 1–16.
1173 doi:10.1038/s41467-018-03619-9

1174 36. Kim H-J, Alonzo ES, Dorothee G, Pollard JW, Sant'Angelo DB.
1175 Selective depletion of eosinophils or neutrophils in mice impacts the
1176 efficiency of apoptotic cell clearance in the thymus. Kim H-J, Alonzo ES,
1177 Dorothee G, Pollard JW, Sant'Angelo DB, editors. PLoS ONE. 2010;5:

1178 e11439. doi:10.1371/journal.pone.0011439.g010

1179 37. Tacke R, Hilgendorf I, Garner H, Waterborg C, Park K, Nowyhed H, et
1180 al. The transcription factor NR4A1 is essential for the development of a
1181 novel macrophage subset in the thymus. Sci Rep. 2015;5: 10055.
1182 doi:10.1038/srep10055

1183 38. Gautier EL, Shay T, Miller J, Greter M, Jakubzick C, Ivanov S, et al.
1184 Gene-expression profiles and transcriptional regulatory pathways that
1185 underlie the identity and diversity of mouse tissue macrophages. Nat
1186 Immunol. 2012;13: 1118–1128. doi:10.1038/ni.2419

1187 39. Ingersoll MA, Spanbroek R, Lottaz C, Gautier EL, Frankenberger M,
1188 Hoffmann R, et al. Comparison of gene expression profiles between
1189 human and mouse monocyte subsets. Blood. 2010;115: e10–e19.
1190 doi:10.1182/blood-2009-07-235028

1191 40. Wang H, Breed ER, Lee YJ, Qian LJ, Jameson SC, Hogquist KA.
1192 Myeloid cells activate iNKT cells to produce IL-4 in the thymic medulla.
1193 Proc Natl Acad Sci. National Academy of Sciences; 2019;116: 22262–
1194 22268. doi:10.1073/pnas.1910412116

1195 41. Chan CT, Fenn AM, Harder NK, Mindur JE, McAlpine CS, Patel J, et al.
1196 Liver X receptors are required for thymic resilience and T cell output. J
1197 Exp Med. 2020;217: 245–23. doi:10.1084/jem.20200318

1198 42. Wada H, Masuda K, Satoh R, Kakugawa K, Ikawa T, Katsura Y, et al.
1199 Adult T-cell progenitors retain myeloid potential. Nature. Nature
1200 Publishing Group; 2008;452: 768–772. doi:10.1038/nature06839

1201 43. Bell JJ, Bhandoola A. The earliest thymic progenitors for T cells
1202 possess myeloid lineage potential. Nature. 2008;452: 764–767.
1203 doi:10.1038/nature06840

1204 44. Schlenner SM, Madan V, Busch K, Tietz A, LAufle C, Costa C, et al.
1205 Fate Mapping Reveals Separate Origins of T Cells and Myeloid
1206 Lineages in the Thymus. Immunity. Elsevier Ltd; 2010;32: 426–436.
1207 doi:10.1016/j.immuni.2010.03.005

1208 45. Witmer-Pack MD, Hughes DA, Schuler G, Lawson L, McWilliam A,
1209 Inaba K, et al. Identification of macrophages and dendritic cells in the
1210 osteopetrotic (op/op) mouse. J Cell Sci. 1993;104 (Pt 4): 1021–1029.

1211 46. Sasmono RT, Oceandy D, Pollard JW, Tong W, Pavli P, Wainwright BJ,
1212 et al. A macrophage colony-stimulating factor receptor-green
1213 fluorescent protein transgene is expressed throughout the mononuclear
1214 phagocyte system of the mouse. Blood. American Society of
1215 Hematology; 2003;101: 1155–1163. doi:10.1182/blood-2002-02-0569

1216 47. Hume DA. Applications of myeloid-specific promoters in transgenic mice
1217 support in vivo imaging and functional genomics but do not support the
1218 concept of distinct macrophage and dendritic cell lineages or roles in

1219 immunity. Journal of Leukocyte Biology. 2011;89: 525–538.
1220 doi:10.1189/jlb.0810472

1221 48. Taniuchi I, Osato M, Egawa T, Sunshine MJ, Bae SC, Komori T, et al.
1222 Differential requirements for Runx proteins in CD4 repression and
1223 epigenetic silencing during T lymphocyte development. Cell. 2002;111:
1224 621–633. doi:10.1016/s0092-8674(02)01111-x

1225 49. Ebihara T, Song C, Ryu SH, Plougastel-Douglas B, Yang L, Levanon D,
1226 et al. Runx3 specifies lineage commitment of innate lymphoid cells. Nat
1227 Immunol. Nature Publishing Group; 2015;16: 1124–1133.
1228 doi:10.1038/ni.3272

1229 50. Fainaru O, Woolf E, Lotem J, Yarmus M, Brenner O, Goldenberg D, et
1230 al. Runx3 regulates mouse TGF-beta-mediated dendritic cell function
1231 and its absence results in airway inflammation. EMBO J. John Wiley &
1232 Sons, Ltd; 2004;23: 969–979. doi:10.1038/sj.emboj.7600085

1233 51. Kohyama M, Ise W, Edelson BT, Wilker PR, Hildner K, Mejia C, et al.
1234 Role for Spi-C in the development of red pulp macrophages and splenic
1235 iron homeostasis. Nat Immunol. Nature Publishing Group; 2008;457:
1236 318–321. doi:10.1038/nature07472

1237 52. Haldar M, Kohyama M, So AY-L, KC W, Wu X, Briseño CG, et al.
1238 Heme-Mediated SPI-C Induction Promotes Monocyte Differentiation into
1239 Iron-Recycling Macrophages. Cell. Elsevier Inc; 2014;156: 1223–1234.
1240 doi:10.1016/j.cell.2014.01.069

1241 53. Yona S, Kim K-W, Wolf Y, Mildner A, Varol D, Breker M, et al. Fate
1242 Mapping Reveals Origins and Dynamics of Monocytes and Tissue
1243 Macrophages under Homeostasis. Immunity. Elsevier; 2013;38: 79–91.
1244 doi:10.1016/j.immuni.2012.12.001

1245 54. McCaughtry TM, Wilken MS, Hogquist KA. Thymic emigration revisited.
1246 J Exp Med. 2007;204: 2513–2520. doi:10.1084/jem.20070601

1247 55. Lienenklaus S, Cornitescu M, Ziętara N, Łyszkiewicz M, Gekara N,
1248 Jabłónska J, et al. Novel reporter mouse reveals constitutive and
1249 inflammatory expression of IFN-beta in vivo. J Immunol. American
1250 Association of Immunologists; 2009;183: 3229–3236.
1251 doi:10.4049/jimmunol.0804277

1252 56. Otero DC, Baker DP, David M. IRF7-dependent IFN-β production in
1253 response to RANKL promotes medullary thymic epithelial cell
1254 development. J Immunol. American Association of Immunologists;
1255 2013;190: 3289–3298. doi:10.4049/jimmunol.1203086

1256 57. Breed ER, Lee ST, Hogquist KA. Directing T cell fate: How thymic
1257 antigen presenting cells coordinate thymocyte selection. Seminars in
1258 Cell and Developmental Biology. Elsevier Ltd; 2017;: 1–9.
1259 doi:10.1016/j.semcdb.2017.07.045

58. Kurd NS, Lutes LK, Yoon J, Chan SW, Dzhagalov IL, Hoover AR, et al. A role for phagocytosis in inducing cell death during thymocyte negative selection. eLife. 2019;8: 1879–18. doi:10.7554/eLife.48097

59. Morioka S, Perry JSA, Raymond MH, Medina CB, Zhu Y, Zhao L, et al. Efferocytosis induces a novel SLC program to promote glucose uptake and lactate release. Nature. Springer US; 2018;563: 1–21. doi:10.1038/s41586-018-0735-5

60. Bleriot C, Chakarov S, Ginhoux F. Determinants of Resident Tissue Macrophage Identity and Function. Immunity. Elsevier Inc; 2020;52: 957–970. doi:10.1016/j.immuni.2020.05.014

61. Stritesky GL, Xing Y, Erickson JR, Kalekar LA, Wang X, Mueller DL, et al. Murine thymic selection quantified using a unique method to capture deleted T cells. Proc Natl Acad Sci. 2013;110: 4679–4684. doi:10.1073/pnas.1217532110

62. Baba T, Nakamoto Y, Mukaida N. Crucial Contribution of Thymic Sirp + Conventional Dendritic Cells to Central Tolerance against Blood-Borne Antigens in a CCR2-Dependent Manner. J Immunol. 2009;183: 3053–3063. doi:10.4049/jimmunol.0900438

63. Gallegos AM, Bevan MJ. Central Tolerance to Tissue-specific Antigens Mediated by Direct and Indirect Antigen Presentation. J Exp Med. 2004;200: 1039–1049. doi:10.1084/jem.20041457

64. Koble C, Kyewski B. The thymic medulla: a unique microenvironment for intercellular self-antigen transfer. J Exp Med. 2009;206: 1505–1513. doi:10.1084/jem.20082449

65. Vobořil M, Brabec T, Dobeš J, Šplíchalová I, Březina J, Čepková A, et al. Toll-like receptor signaling in thymic epithelium controls monocyte-derived dendritic cell recruitment and Treg generation. Nature Communications. Springer US; 2020;11: 1–16. doi:10.1038/s41467-020-16081-3

66. Dixit VD. Impact of immune-metabolic interactions on age-related thymic demise and T cell senescence. Semin Immunol. Elsevier Ltd; 2012;24: 321–330. doi:10.1016/j.smim.2012.04.002

67. Rivera-Gonzalez GC, Shook BA, Andrae J, Holtrup B, Bollag K, Betsholtz C, et al. Skin Adipocyte Stem Cell Self-Renewal Is Regulated by a PDGFA/AKT-Signaling Axis. Stem Cell. Elsevier Inc; 2016;19: 738–751. doi:10.1016/j.stem.2016.09.002

68. Olson LE, Soriano P. Increased PDGFRα Activation Disrupts Connective Tissue Development and Drives Systemic Fibrosis. Developmental Cell. Elsevier Ltd; 2009;16: 303–313. doi:10.1016/j.devcel.2008.12.003

69. Satpathy AT, KC W, Albring JC, Edelson BT, Kretzer NM, Bhattacharya

1301 D, et al. Zbtb46expression distinguishes classical dendritic cells and
1302 their committed progenitors from other immune lineages. J Exp Med.
1303 2012;209: 1135–1152. doi:10.1084/jem.20120030

1304 70. Guilliams M, Mildner A, Yona S. Developmental and Functional
1305 Heterogeneity of Monocytes. Immunity. Elsevier Inc; 2018;49: 595–613.
1306 doi:10.1016/j.immuni.2018.10.005

1307 71. Tabula Muris Consortium. Single-cell transcriptomics of 20 mouse
1308 organs creates a Tabula Muris. Nature. Nature Publishing Group;
1309 2018;562: 367–372. doi:10.1038/s41586-018-0590-4

1310 72. Han X, Wang R, Zhou Y, Fei L, Sun H, Lai S, et al. Mapping the Mouse
1311 Cell Atlas by Microwell-Seq. Cell. Elsevier Inc; 2018;172: 1091–
1312 1097.e17. doi:10.1016/j.cell.2018.02.001

1313 73. Tabula Muris Consortium. A single-cell transcriptomic atlas
1314 characterizes ageing tissues in the mouse. Nature. Nature Publishing
1315 Group; 2020;583: 590–595. doi:10.1038/s41586-020-2496-1

1316 74. Kernfeld EM, Genga RMJ, Neherin K, Magaletta ME, Xu P, Maehr R. A
1317 Single-Cell Transcriptomic Atlas of Thymus Organogenesis Resolves
1318 Cell Types and Developmental Maturation. Immunity. Elsevier Inc;
1319 2018;: 1–33. doi:10.1016/j.immuni.2018.04.015

1320 75. Park J-E, Botting RA, Domínguez Conde C, Popescu D-M, Lavaert M,
1321 Kunz DJ, et al. A cell atlas of human thymic development defines T cell
1322 repertoire formation. Science. American Association for the
1323 Advancement of Science; 2020;367: eaay3224–12.
1324 doi:10.1126/science.aay3224

1325 76. Bornstein C, Nevo S, Giladi A, Kadouri N, Pouzolles M, Gerbe F, et al.
1326 Single-cell mapping of the thymic stroma identifies IL-25-producing tuft
1327 epithelial cells. Nature. Springer US; 2018;559: 1–25.
1328 doi:10.1038/s41586-018-0346-1

1329 77. Bautista JL, Cramer NT, Miller CN, Chavez J, Berrios DI, Byrnes LE, et
1330 al. Single-cell transcriptional profiling of human thymic stroma uncovers
1331 novel cellular heterogeneity in the thymic medulla. Nature
1332 Communications. Nature Publishing Group; 2021;12: 1096–15.
1333 doi:10.1038/s41467-021-21346-6

1334 78. Burnett SH, Kershen EJ, Zhang J, Zeng L, Straley SC, Kaplan AM, et
1335 al. Conditional macrophage ablation in transgenic mice expressing a
1336 Fas-based suicide gene. Journal of Leukocyte Biology. Society for
1337 Leukocyte Biology; 2004;75: 612–623. doi:10.1189/jlb.0903442

1338 79. Jung S, Aliberti J, Graemmel P, Sunshine MJ, Kreutzberg GW, Sher A,
1339 et al. Analysis of fractalkine receptor CX(3)CR1 function by targeted
1340 deletion and green fluorescent protein reporter gene insertion. Mol Cell
1341 Biol. 2000;20: 4106–4114.

80. Lindquist RL, Shakhar G, Dudziak D, Wardemann H, Eisenreich T, Dustin ML, et al. Visualizing dendritic cell networks in vivo. Nat Immunol. 2004;5: 1243–1250. doi:10.1038/ni1139

81. Faust N, Varas F, Kelly LM, Heck S, Graf T. Insertion of enhanced green fluorescent protein into the lysozyme gene creates mice with green fluorescent granulocytes and macrophages. Blood. 2000;96: 719–726.

82. Roesch K, Jadhav AP, Trimarchi JM, Stadler MB, Roska B, Sun BB, et al. The transcriptome of retinal Müller glial cells. J Comp Neurol. 2008;509: 225–238. doi:10.1002/cne.21730

83. Madisen L, Zwingman TA, Sunkin SM, Oh SW, Zariwala HA, Gu H, et al. A robust and high-throughput Cre reporting and characterization system for the whole mouse brain. Nature Neuroscience. Nature Publishing Group; 2009;13: 133–140. doi:10.1038/nn.2467

84. Picelli S, Faridani OR, rklund ASKBO, Winberg GOS, Sagasser S, Sandberg R. Full-length RNA-seq from single cells using Smart-seq2. Nature Protocols. Nature Publishing Group; 2014;9: 171–181. doi:10.1038/nprot.2014.006

85. Picelli S, Björklund ÅK, Faridani OR, Sagasser S, Winberg G, Sandberg R. Smart-seq2 for sensitive full-length transcriptome profiling in single cells. Nat Meth. 2013;10: 1096–1098. doi:10.1038/nmeth.2639

86. Love MI, Huber W, Anders S. Moderated estimation of fold change and dispersion for RNA-seq data with DESeq2. Genome Biol. BioMed Central; 2014;15: 31–21. doi:10.1186/s13059-014-0550-8

87. Schmeier S, Alam T, Essack M, Bajic VB. TcoF-DB v2: update of the database of human and mouse transcription co-factors and transcription factor interactions. Nucleic Acids Res. 2017;45: D145–D150. doi:10.1093/nar/gkw1007

88. Reich M, Liefeld T, Gould J, Lerner J, Tamayo P, Mesirov JP. GenePattern 2.0. Nat Genet. Nature Publishing Group; 2006;38: 500–501. doi:10.1038/ng0506-500

89. Yu G, Wang L-G, Han Y, He Q-Y. clusterProfiler: an R Package for Comparing Biological Themes Among Gene Clusters. OMICS: A Journal of Integrative Biology. Mary Ann Liebert, Inc., publishers; 2012;16: 284–287. doi:10.1089/omi.2011.0118

90. Heyne GW, Plisch EH, Melberg CG, Sandgren EP, Peter JA, Lipinski RJ. A Simple and Reliable Method for Early Pregnancy Detection in Inbred Mice. J Am Assoc Lab Anim Sci. 2015;54: 368–371.

91. Iturri L, Saenz Coronilla J, Lallemand Y, Gomez Perdiguero E. Identification Of Erythromyeloid Progenitors And Their Progeny In The Mouse Embryo By Flow Cytometry. JoVE. 2017;: 1–10.

1383 doi:10.3791/55305

1384 92. Wolf FA, Angerer P, Theis FJ. SCANPY: large-scale single-cell gene
1385 expression data analysis. Genome Biol. BioMed Central; 2018;19: 15–
1386 5. doi:10.1186/s13059-017-1382-0

1387 93. Polański K, Young MD, Miao Z, Meyer KB, Teichmann SA, Park J-E.
1388 BBKNN: fast batch alignment of single cell transcriptomes.
1389 Bioinformatics. 2019;36: 964–965.
1390 doi:10.1093/bioinformatics/btz625#supplementary-data

1391 94. McInnes L, Healy J, Melville J. UMAP: Uniform Manifold Approximation
1392 and Projection for Dimension Reduction. ArXiv e-prints. 2018.
1393 doi:1802.03426v3

1394

1395 **Acknowledgments**

1396 We are grateful to the IMMGEN consortium for performing the RNA
1397 sequencing of our samples and providing access to its database. We thank
1398 the following core facilities at National Yang-Ming Chiao-Tung University:
1399 Instrumentation Resource Center for providing access to its sorting and
1400 imaging facility and the Animal Facility for mouse husbandry. We are very
1401 grateful to Wan-Chun Chang, Bing-Xiu Guo, Chien-Yi Tung, and Kate Hua
1402 from the Genomics Center for Clinical and Biotechnological Applications of
1403 NCFB (NYCU, Taipei) for help with scRNA-Seq. Special thanks go to Dr.
1404 Fang Liao, Academia Sinica, Taipei, for help with cell sorting and for providing
1405 the 24G2 hybridoma, and Chang-Feng Chu for technical assistance. We are
1406 very grateful to Ms. Su-Hua Jiang at Veterans General Hospital, Taipei, for
1407 help with using the irradiator. Some figures were made with BioRender.

1408 This work was supported by the Ministry of Science and Technology
1409 (grants # 106-2320-B-010 -026 -MY3, and 107-2320-B-010 -016 -MY3 to IL
1410 Dzhagalov and grants # 107-2320-B-010-020, and 108-2628-B-010-005 to CL

1411 Hsu), the Yen-Tjing Ling Medical Foundation (grants # CI-107-6 and CI-108-5
1412 to IL Dzhagalov), and the Cancer Progression Research Center (NYCU). The
1413 authors declare no competing financial interests.

1414 **Author contributions**

1415 TA Zhou designed experiments, performed research, analyzed and
1416 interpreted data, and wrote the manuscript; HP Hsu and CY Lin performed
1417 research, analyzed and interpreted data; YH Tu and HC Huang analyzed the
1418 scRNA-Seq data; NJ Chen, JW Tsai, EA Robey, and CL Hsu provided
1419 expertise, shared critical reagents, and edited the manuscript; IL Dzhagalov
1420 conceptualized the studies, designed experiments, performed research,
1421 analyzed, interpreted the data, and wrote the manuscript.

1422

Supplementary figures and tables

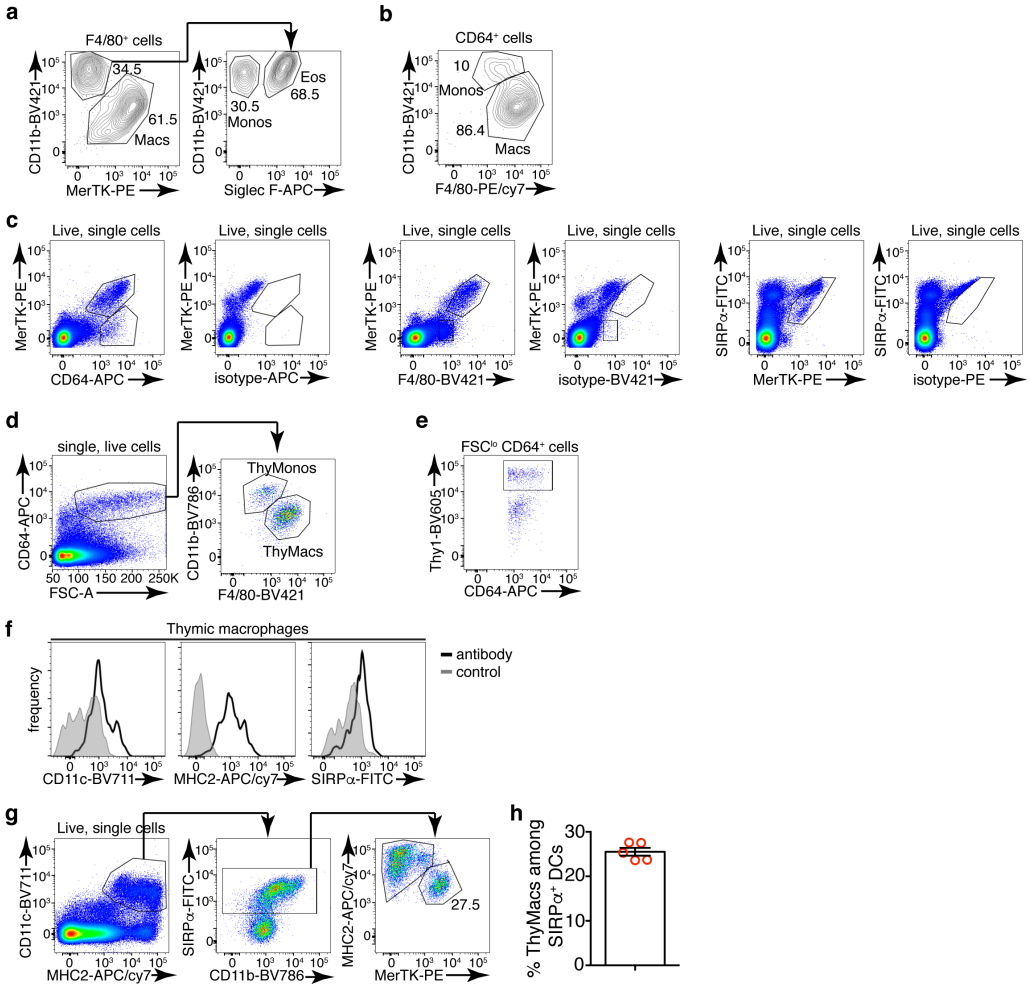

Figure 1 – Figure supplement 1: Phenotype of thymic macrophages and other myeloid cells positive for F4/80 and CD64. a Example flow cytometry plots breaking down F4/80$^+$ cells in the thymus into macrophages (MerTK$^+$), eosinophils (CD11b$^+$MerTK$^-$Siglec F$^+$) and monocytes (CD11b$^+$MerTK$^-$Siglec F$^-$). **b** An example flow cytometry plot dividing CD64+ cells into macrophages (F4/80$^+$CD11b^{lo}) and monocytes (CD11b$^+$F4/80^{lo}). **c** Representative flow cytometry staining of enzymatically digested thymus single-cell suspension for CD64, MerTK, and F4/80 and respective isotype controls. **d** Gating strategy routinely used to identify thymic macrophages as CD64$^+$F4/80$^+$CD11b^{lo}FSC^{hi} cells. **e** Example flow cytometry plots showing that

1435 CD64^{+}FSC^{lo} cells include Thy1^{+} cells (most likely thymocytes). **f** Expression of

1436 CD11c, MHC2, and SIRPα on ThyMacs with respective controls. **g** Example

1437 flow cytometry plots showing that gating on CD11c^{+}MHC2^{+} thymus cells, in

1438 addition to DCs, also includes macrophages, especially among SIRPα^{+} cells.

1439 **h** Frequency of MerTK^{+} cells among CD11c^{+}MHC2^{+}SIRPα^{+} cells. The data

1440 are mean±SEM from 5 individual mice. Each dot is an individual mouse. The

1441 flow cytometry plots are representative of ≥5 individual experiments.

1442

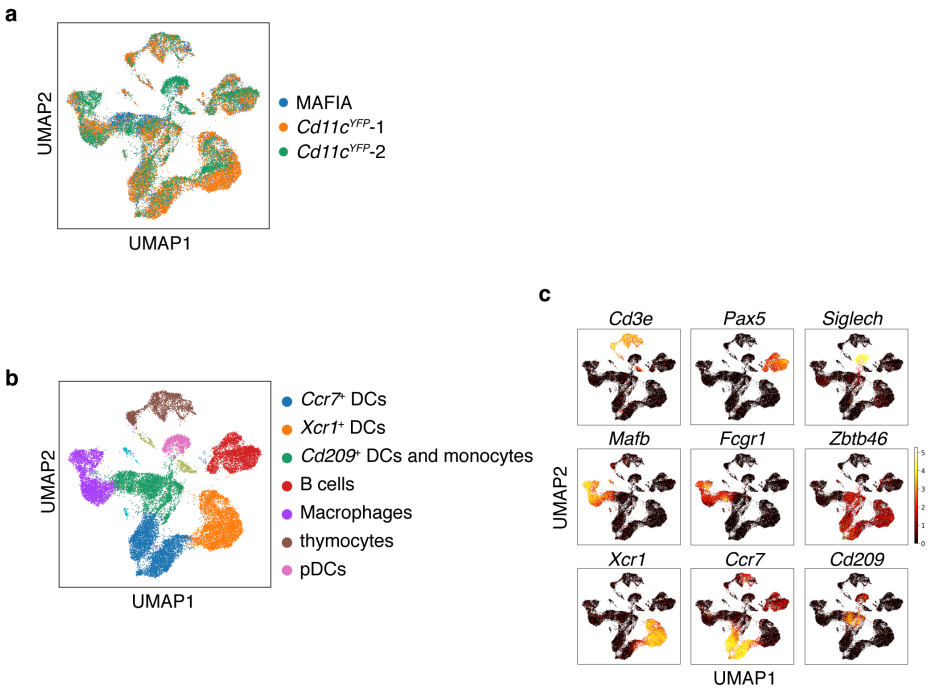

1443 **Figure 1 – Figure Supplement 2: UMAP clustering of single-cell RNA-**

1444 **Sequencing (scRNA-Seq) data. a** Clustering of the scRNA-Seq data shows

1445 that the cells from the three samples (one from GFP^{+} cells in MAFIA mice and

1446 two from YFP^{+} cells in *Cd11c^{YFP}* mice) overlap considerably. **b** Identification of

1447 the clusters from the scRNA-Seq data based on lineage-specific markers. **c**

1448 Expression of lineage-specific markers in different clusters.

1449

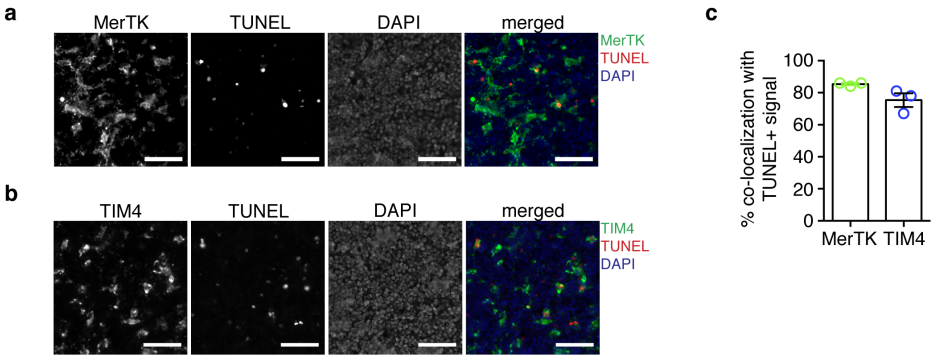

1450 **Figure 1 – Figure Supplement 3: Most TUNEL⁺ apoptotic cells co-**

1451 **localize with thymic macrophages. a** Example images showing co-

1452 localization of TUNEL⁺ apoptotic cells and MerTK⁺ ThyMacs. **b** Example

1453 images showing co-localization of TUNEL⁺ apoptotic cells and TIM4⁺

1454 ThyMacs. Scale bars in **a** and **b** are 50 μm. **c** Frequencies of the co-

1455 localization of TUNEL⁺ signal with MerTK⁺ and TIM4⁺ cells. All

1456 immunofluorescent images are representative of at least 3 independent

1457 repeats. Data in **c** represent mean±SEM. Each dot is an individual mouse.

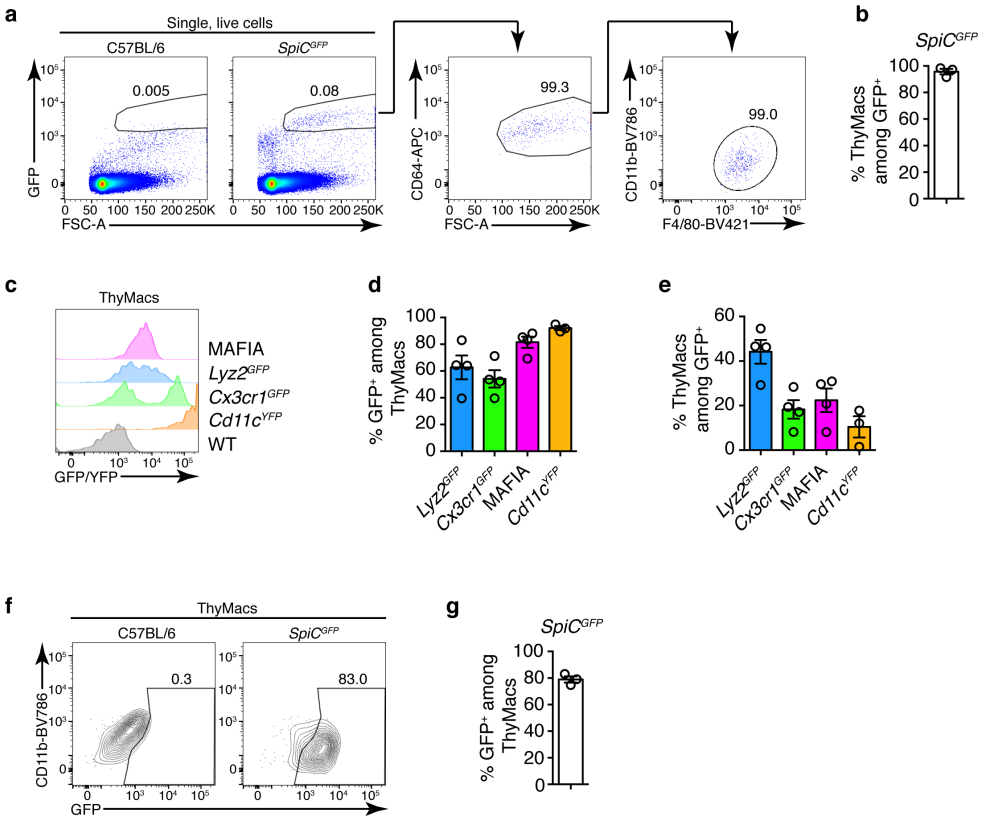

1458 **Figure 2 – Figure Supplement 1: Expression of *Spic*^{GFP} marks most**
1459 **thymic macrophages. a** Example of the gating strategy to identify ThyMacs
1460 among *Spic*$^{GFP+}$ cells. **b** Frequencies of ThyMacs among *Spic*$^{GFP+}$ cells. **c**
1461 Representative flow cytometry plots of the expression of four reporter alleles
1462 in ThyMacs. **d** Frequencies of GFP/YFP^{+} cells among ThyMacs. **e**
1463 Frequencies of ThyMacs among GFP/YFP^{+} cells. **f** Representative flow
1464 cytometry plots of the expression of *Spic*^{GFP} in ThyMacs. **g** Frequencies of
1465 *Spic*$^{GFP+}$ cells among ThyMacs. All flow cytometry plots are representative of
1466 at least 3 independent repeats. Data in **b**, **d**, **e**, and **f** represent mean±SEM.
1467 Each dot is an individual mouse. The numbers in the flow cytometry plots are
1468 the percent of cells in the respective gate.
1469

Table S1: E**xpression of differentially up-regulated transcription factors in thymic macrophages**

Gene name	ThyMacs	non-ThyMacs
Irf7	3879.32	300.82
Irf8	3528.27	1474.35
Stat1	2403.69	522.04
Dnmt3a	1515.94	647.81
Znxf1	1379.89	635.36
Stat2	1210.35	472.53
Nr1h3	1182.17	147.05
Srebf1	975.09	399.06
Rxra	760.26	298.55
Trps1	746.36	232.48
Runx3	723.14	9.76
Relb	715.53	293.92
Sp100	696.94	324.47
Zbp1	639.19	69.83
Tfec	588.72	74.66
Spic	573.11	34.36
Nfkbie	569.74	226.76
Ncoa4	550.69	249.15
Rest	548.22	269.22
Meis3	530.8	120.91
Bhlhe40	490.59	99.56
Parp12	414.11	126.82
Arid5b	374.03	177.08
Creb5	295.14	47.91
Pparg	276.54	33.24

1470 **Figure 2 – Table Supplement 1: Expression of differentially up-**
1471 **regulated transcription factors in thymic macrophages.** Transcription
1472 factors that were highly expressed in thymic macrophages (>250) and up-

1473 regulated >2-fold in thymic macrophages compared to non-thymic
1474 macrophages were listed alphabetically, and the geometric mean of 4
1475 replicates of thymic macrophages (ThyMacs) and two replicates of each of the
1476 9 non-thymic macrophage populations (non-ThyMacs) were recorded. Non-
1477 thymic macrophages are: spleen red pulp macrophages, Kupffer cells,
1478 bronchoalveolar lavage macrophages, peritoneal cavity macrophages, aorta
1479 macrophages, heart macrophages, white adipose tissue macrophages,
1480 central nervous system microglia, spinal cord macrophages.

Table S2. **List of the differentially expressed genes among *Timd*4+ thymic macrophages, *Cx3cr1*+ thymic macrophages, and thymic monocytes**

CX3CR1+ ThyMacs		**Tim4+ ThyMacs**		**ThyMonos**	
Gene name	adjusted p-value	Gene name	adjusted p-value	Gene name	adjusted p-value
Ctsz	0	*Hpgd*	0	*Alox5ap*	0
Cd63	0	*Serpinb6a*	0	*S100a6*	0
Pmepa1	0	*Slc40a1*	0	*Ly6c2*	0
Zmynd15	0	*Cd81*	0	*Ifi27l2a*	0
Olfml3	0	*Vcam1*	0	*Fau*	0
Mmp2	0	*Cfp*	0	*Coro1a*	0
AU020206	1.60E-290	*Spic*	0	*Ccr2*	0
Plxnd1	1.59E-285	*Trf*	0	*Rps27*	0
Cst7	8.68E-279	*Actn1*	0	*Tmsb10*	0
Dnase1l3	2.45E-270	*Maf*	0	*Ifitm2*	7.21E-302
Timp2	2.15E-267	*Pld3*	0	*Fxyd5*	6.36E-299
Lgals3bp	8.69E-263	*Il18*	0	*Rps19*	2.04E-292
Pdgfa	6.87E-255	*Mrc1*	0	*Rpl18*	6.50E-291
Mmp14	2.33E-253	*Crip2*	0	*Rpl9*	1.11E-289
Fam46c	9.99E-235	*Tmem65*	0	*Rps23*	1.28E-289
Chst2	1.19E-226	*Igf1*	0	*Napsa*	8.91E-279
Cp	5.36E-225	*Epb41l3*	0	*Ms4a4c*	8.25E-272
Camk1	7.12E-225	*Timd4*	0	*Plac8*	2.10E-270
B2m	1.09E-222	*Blvrb*	0	*Rpl18a*	9.26E-269
Lhfpl2	4.52E-217	*Clec1b*	0	*S100a4*	4.98E-268
Acp5	5.90E-216	*Cd68*	0	*Cd52*	3.67E-267
Lag3	3.91E-213	*Axl*	0	*Rps14*	1.94E-266
Lyz2	1.28E-209	*Paqr9*	3.32E-307	*Ifitm3*	3.19E-263
H2-M2	1.22E-199	*Sdc3*	3.45E-305	*Rpl34*	2.02E-261
Psap	7.26E-198	*Myo9a*	5.59E-305	*Rps27a*	3.67E-260
Gatm	1.33E-192	*Scp2*	3.79E-302	*Rpl36*	1.54E-259
Cpd	1.50E-192	*Selenop*	2.10E-295	*Rps16*	2.55E-258

C3	2.34E-187	*Lrp1*	2.08E-294	*Rpl24*	1.37E-257
Cxcl16	8.11E-183	*Lap3*	1.45E-290	*Rps9*	6.34E-253
Lgals3	1.57E-182	*Marcks*	2.77E-279	*Gpr141*	1.21E-246
Ube2j1	1.63E-180	*Glul*	3.64E-279	*Rpl27a*	3.06E-243
Plxnc1	9.84E-180	*Hebp1*	3.76E-278	*Rpl17*	8.15E-241
Stab1	4.07E-176	*Ear2*	4.53E-276	*Rps24*	1.46E-240
Cyth1	3.27E-163	*Apoc1*	2.49E-275	*Rps13*	2.34E-236
Spsb1	3.96E-163	*Kcna2*	3.72E-275	*Rpl38*	1.95E-226
Blnk	2.35E-162	*Myo10*	9.05E-269	*H2-DMb1*	1.02E-223
Cx3cr1	9.29E-162	*Atp13a2*	2.95E-267	*Rps18*	5.39E-223
Med10	5.25E-161	*Slc1a3*	6.24E-263	*Rpl19*	3.68E-221
Nek6	5.28E-160	*Slco2b1*	1.11E-258	*Rpl8*	2.01E-219
Ptms	1.05E-159	*mt-Nd2*	3.45E-258	*Rpl7a*	4.17E-217
Anxa5	1.10E-156	*Wwp1*	2.16E-253	*Gm34084*	5.23E-216
Gpnmb	1.21E-154	*Aplp2*	4.22E-248	*Rpl13*	2.08E-215
Itgb5	2.78E-154	*Atp8a1*	5.03E-248	*Rpl11*	2.47E-213
Myo5a	1.11E-146	*P2ry13*	3.17E-247	*Rpl35a*	2.13E-210
Runx3	1.81E-146	*Ccdc148*	4.70E-245	*Rpsa*	1.62E-209
Tmem176a	2.34E-144	*Grn*	1.58E-244	*Rpl6*	5.70E-208
Ctss	4.81E-141	*Bank1*	1.82E-239	*Tpt1*	2.63E-206
Sh3pxd2b	9.38E-141	*Mertk*	2.15E-238	*Rack1*	2.14E-203
Rtcb	4.42E-140	*Nr1h3*	1.13E-235	*Rpl23*	6.14E-199
Fam20c	1.91E-139	*Prnp*	2.93E-235	*Rpl26*	7.48E-198
Il2rg	8.84E-138	*Ninj1*	2.42E-234	*Rps6*	6.64E-197
Lpcat2	8.53E-137	*Fcna*	3.33E-233	*Rps10*	2.06E-195
Kynu	8.49E-136	*Csrp1*	1.16E-230	*Ier5*	1.06E-191
Tnfsf13b	8.77E-136	*Rgl1*	7.18E-229	*Rps3*	8.23E-185
Gpr157	1.18E-135	*Lpl*	4.94E-223	*Rpl27*	8.23E-185
Tgfbr1	7.63E-135	*Fam213b*	1.08E-222	*Rps5*	8.36E-185
H2-K1	1.15E-133	*Tcf7l2*	1.26E-222	*Rps7*	3.96E-182
Basp1	1.23E-133	*AB124611*	4.64E-221	*Rps15a*	6.82E-182
Pla2g7	1.80E-132	*Abcc3*	3.28E-216	*Rps11*	1.97E-180
Fth1	4.19E-131	*Fcgrt*	5.79E-216	*Rps4x*	5.07E-180
Ggh	1.85E-126	*Tgm2*	1.88E-215	*Rplp0*	3.09E-177
Adam19	6.94E-126	*Itgad*	5.35E-214	*Ly6i*	8.17E-176
C3ar1	7.35E-125	*Ptgs1*	2.94E-213	*S100a11*	6.23E-175
Ccl12	3.37E-123	*Laptm4a*	1.01E-212	*Atox1*	1.22E-174
Hvcn1	2.51E-121	*Comt*	1.33E-206	*Pim1*	9.56E-174
Anxa3	8.60E-121	*Creg1*	3.24E-205	*Sh3bgrl3*	3.97E-173
Tgfbi	1.88E-120	*Adgre1*	9.67E-205	*Ciita*	7.35E-173
Ctsd	2.73E-117	*Clec12a*	6.33E-204	*Eef1a1*	6.09E-172
Itm2c	5.19E-116	*Tspan4*	7.80E-203	*Rps3a1*	9.09E-168
Tmem119	5.62E-116	*Txn1*	9.13E-203	*Gm2a*	6.07E-165
Rap2a	1.03E-114	*Ctsb*	9.52E-201	*Ptprc*	2.05E-163
Ctsl	4.00E-114	*Mrap*	5.65E-197	*Rpl37*	1.51E-161
Itga6	1.83E-113	*Slc16a9*	5.99E-197	*Rps25*	3.03E-160

B4galnt1	2.45E-113	*Abcg3*	3.83E-196	*H3f3a*	5.92E-159
Fam3c	1.64E-112	*Pla2g15*	4.22E-196	*Btg2*	1.14E-158
Tmem173	1.54E-111	*C1qc*	6.17E-192	*Rpl15*	1.42E-158
Ski	3.59E-111	*Agpat3*	1.68E-191	*Cnn2*	1.09E-156
Anpep	5.85E-111	*Hs6st1*	1.95E-191	*Cdkn1a*	2.57E-156
Gng2	2.37E-110	*Dmpk*	2.15E-191	*Slfn1*	4.83E-155
Nceh1	2.88E-110	*Cd38*	1.79E-190	*Sem1*	4.08E-154
H2-Q7	4.94E-108	*Tmem26*	2.02E-189	*Lsp1*	1.34E-152
Rtn1	1.28E-106	*Slc11a1*	1.05E-188	*Rpl37a*	1.78E-152
Sorl1	1.31E-103	*Cd300a*	1.41E-187	*Rpl22*	3.64E-152
Glipr1	1.22E-102	*Slc7a7*	3.28E-187	*Sirpb1c*	4.81E-152
Gsn	2.00E-102	*Cyb5a*	6.94E-187	*Traf1*	6.97E-152
Afdn	4.54E-102	*Sipa1l1*	7.41E-187	*Emb*	4.22E-151
Ak2	1.11E-101	*Il18bp*	1.48E-186	*Rpl30*	1.32E-147
Ntpcr	2.21E-98	*Cd86*	2.52E-183	*Rps15*	1.14E-146
Scarb2	3.16E-97	*Vamp5*	3.05E-183	*H2-Ab1*	2.84E-145
Creb5	5.41E-97	*Jup*	6.69E-182	*Il1b*	3.05E-145
Gsto1	5.56E-97	*Blvra*	1.30E-178	*Rps28*	4.52E-145
Ncf1	4.26E-96	*Mgst1*	6.48E-178	*Jarid2*	1.82E-143
Ppfia4	4.97E-96	*Tbxas1*	1.47E-177	*Rps26*	1.53E-142
Chchd10	7.77E-96	*Hpgds*	2.04E-177	*Rpl32*	4.21E-142
Gna12	1.23E-95	*Tgfbr2*	2.70E-176	*Pld4*	9.07E-142
Mvb12b	1.80E-95	*Clec4n*	3.52E-175	*Cbfa2t3*	1.54E-141
Rasal3	1.45E-94	*Ms4a7*	5.30E-175	*Rps21*	4.04E-141
Scoc	6.86E-94	*Sirpa*	3.35E-171	*Fgr*	4.04E-141
Cfb	6.00E-93	*Fyn*	2.84E-168	*Rps8*	1.11E-139
Lmna	1.04E-92	*Cadm1*	2.20E-167	*Cd74*	5.34E-138

Figure 5 – Table Supplement 1: List of the differentially expressed genes among *Timd4*$^+$ thymic macrophages, *Cx3cr1*$^+$ thymic macrophages, and thymic monocytes. The top 100 differentially expressed genes among the three clusters are listed by their negative $\log_{10}$ transformed p-value.